Physics of the Earth and Planetary Interiors 294 (2019) 106277

Contents lists available at ScienceDirect

Physics of the Earth and Planetary Interiors

journal homepage: www.elsevier.com/locate/pepi

Source characteristics of the NW Himalaya and its adjoining region: Geodynamical implications

Vandana*, O.P. Mishra

National Centre for Seismology, Ministry of Earth Sciences, New Delhi, India

ARTICLE INFO

Keywords:
Source parameters
Brune model
Stress drop
Corner frequency
Kappa
Geodynamics

ABSTRACT

In this study, we propose a novel interpretation of source parameters estimated using Brune model for the NW Himalaya and its adjoining region. Analysis of 157 events ($2.2 \le Mw \le 4.9$) resulted in the scaling relationship between seismic moment (M_0) and corner frequency (f_c) for the region as: $M_0 = 8 \times 10^{22} fc^{-2.89}$, which is in good unison to the Garhwal and the Kumaon Himalaya with analogous seismogenic potential. Variability of Kappa (0.01 s - 0.08 s) with varying number of events ($2.5 \le M \le 5.0$) at different depths is indicative of nature and extent of structural heterogeneity beneath the source zone, which controls the propensity of background seismicity that provides enough testimony to complex geodynamical set-up of the NW Himalaya and its adjoining region.

Source radii of source zone varying from 148 m to 975 m with static stress drops calculated for a given constant stress of 0.1 bar, 1 bar, 10 bar and 100 bar correspond to an average stress drop varied from 0.4 bar to 99.9 bar. Seismic moments of events vary from 2.64×10^{19} dyne-cm to 2.32×10^{23} dyne-cm with increase of the source radii. We infer that variability in stress drop ($\Delta\sigma$) for seismic moment (M_o) is attributed to different seismic sources of varying strengths associated with different structural heterogeneities. Stress drop ($\Delta\sigma$) of the events has good correspondence with source depth, having the linear relationship of shear stress regime in the brittle crust with stress drop ($\Delta\sigma$) and source depth, suggesting the presence of intricate subsurface seismogenic sources beneath the NW Himalaya and its adjoining region.

1. Introduction

The knowledge of source parameters is required to map the seismotectonics sources, which form an important ingredient for seismic hazard assessment. Applications of earthquake source parameters involve mapping of tectonic stress from the space-time variation of stress drops, developing scaling laws, quantifying the excitation of high frequency strong ground motion, and distinguishing nuclear explosions from earthquakes that help to understand the seismogenesis of the study region. Since the seminal works of Aki (1967) and Brune (1970), significant investigations have been carried out in the estimation of source parameters, and development of scaling laws to study the relationship of earthquake source spectrum with magnitudes and other source parameters (Tucker and Brune, 1977, Fletcher, 1980, Archuleta et al., 1982, Hanks and Boore, 1984, O'Neill, 1984, Andrews, 1986, Abercrombie and Leary, 1993, Gupta and Rambabu, 1993, Sharma and Wason, 1994, Kumar et al., 1994, Zobin and Havskov, 1995, Bansal, 1998, Mandal and Rastogi, 1998, Kumar et al. 2006, 2012a, b, 2013a, b, 2014a, b, Paidi et al., 2015, Parshad et al., 2014, Kumar et al., 2015). There are several methodologies, which have been applied to estimate source characterisation of the earthquake. Aki (1967) developed a scaling law to represent the variation of amplitude spectrum of seismic source with magnitude. One of the models developed as ω^3 model, and another is called ω^2 model. The ω^2 model was obtained by fitting an exponentially decaying function to the autocorrelation function of dislocation velocity. The spectra are also calibrated with surface wave magnitude (Ms). Previous studies concluded that ω^2 model of Aki (1967) agrees with observations on assumption of self-similarity and helped in the development of scaling law between amplitude of source and source parameters, but ω^3 model does not bear observational constraints. Brune (1970, 1971) gave a circular fault model in which application of tangential stress pulse instantaneously to the interior of a dislocation surface generates shear wave that propagates perpendicularly to the fault plane. Subsequently, based on ω^2 model, Brune (1970, 1971) has developed a comprehensive concept that found applicable to both near and far field displacement time functions and spectra. This model considered the effect of fractional stress drop on the spectrum, which is considered as a base for source characterisation of the NW Himalaya and its adjoining region.

To estimate the source parameters, a series of studies based on spectral analysis were made by different researchers (Hanks, 1982, Papageorgiou and Aki, 1983a, 1983b, Anderson and Hough, 1984,

* Corresponding author.
E-mail addresses: vandana.ghangas@gmail.com (Vandana), omp.mishra@nic.in (O.P. Mishra).

https://doi.org/10.1016/j.pepi.2019.106277
Received 1 January 2019; Received in revised form 14 June 2019; Accepted 18 June 2019
Available online 03 July 2019
0031-9201/

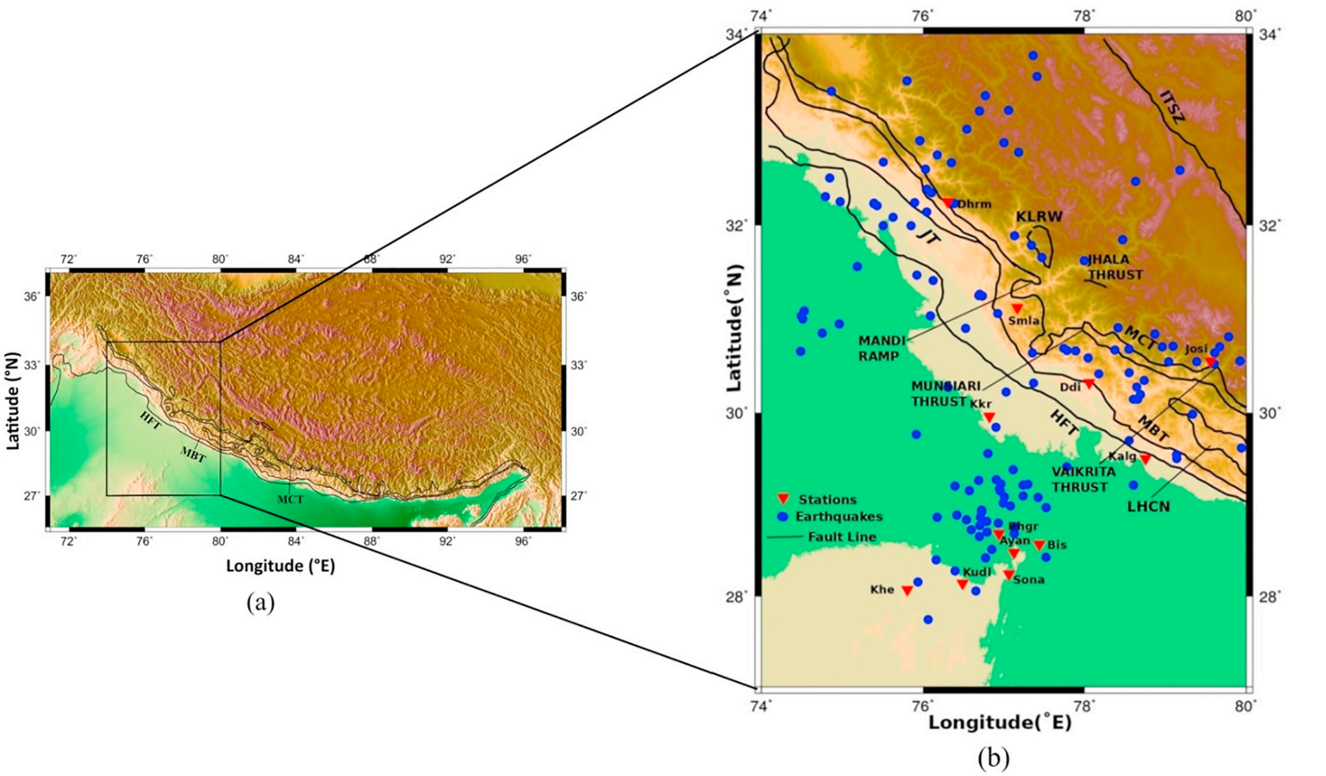

Fig. 1. a: Map of the entire Himalayan range with the study region (the NW Himalaya and its adjoining region) (rectangular box). Fig. 1b: Map showing tectonic features of the NW Himalaya and its adjoining region with tectonic features shown by lines marked as: Main Boundary Thrust (MBT), Main Central Thrust (MCT), Himalayan Frontal Thrust (HFT), Munsiari thrust, Vaikrita thrust, Jammu thrust (JT), Lesser Himalayan Crystalline Nappe (LHCN), Kullu-Larji-Rampur Window (KLRW), Jhala thrust. Filled triangles depict the network stations and filled circles represent the relocated epicentres of 157 events.

Anderson, 1986, 1991). These studies show that the acceleration spectra of earthquakes are limited to a frequency band between corner frequency and f_{max}. Essentially f_{max} represents the high frequency cut-off beyond which acceleration spectra decays sharply. Using the Oroville aftershocks data, Hanks (1982) estimated f_{max} at different stations and found that f_{max} for stations located on alluvium are different from those located on bedrocks. Later on, Papageorgiou and Aki (1983a, 1983b) suggested that f_{max} is attributing to the size of a cohesive zone and from earthquake engineering perspective f_{max} is an important parameter as it controls the level of high frequency strong ground motion. Previous studies done by Anderson and Hough (1984) and Anderson (1986, 1991) related to high-cut fall off near-surface attenuation, but a recent study by Purvance and Anderson (2003) shows that the high-cut fall-off is primarily controlled by source characteristics as opposed to propagation path effects. Many studies have been demonstrated that the fall off of high frequencies in the acceleration spectrum can be attributed to source or site effects (Hanks, 1982; Papageorgiou and Aki, 1983a, 1983b; Campillo, 1983; Anderson and Hough, 1984; Anderson, 1986, 1991; Faccioli, 1986; Aki, 1987; Papageorgiou, 1988; Fujiwara and Irikura, 1991; Yokoi and Irikura, 1991; Kinoshita, 1992; Morikawa and Sasatani, 2000; Tsai and Chen, 2000; Purvance and Anderson, 2003; Kumar et al., 2012a, b, 2013a, 2013b, c, Kumar et al., 2014a, b).

In the present study, the spectral parameters such as low frequency spectral level (Ω_0), corner frequency (f_c), high-cut frequency (f_{max}), roll-off of high frequency acceleration spectrum above f_{max} (p) and near surface attenuation factor Kappa (κ) for the NW Himalaya and its adjoining parts have been estimated which are very intricate but intriguing to understand the complexity in seimogenesis. These spectral parameters utilized to estimate the source parameters viz. seismic moments (M_o), source radii (r), stress drops ($\Delta\sigma$) and moment magnitudes (M_w), have been studied using data of 157 events ($2.2 \le Mw \le 4.9$) that occurred between Jan 2009 and Dec 2017 for the study region. The spectral and source parameters have been estimated using the processing tool of Kumar et al. (2012a, b) that highlights the geodynamical aspects of the NW Himalaya and its adjoining parts.

2. Geology and seismotectonics

The Himalaya is one of the most prominent and active intra-continental orogens showing a classical example of topographic relief development in a compressional tectonic setting. The origin of Himalaya is attributed to the collision of the Indian plate with the Eurasian plate, starting about 50 Ma and persistent convergence that caused a shortening of about 2000–3000 km thereafter (Valdiya 1998). Recent studies put forth a series of intriguing geotectonic evidence to show the subduction of the Indian plate beneath the Tibetan Plateau (Huang and Dapeng, 2006, Zhou and Lei 2016, He Ping et al., 2018). From south to north the Himalaya is divided into four major tectonic and physiographic belts namely, the Sub Himalaya (Siwalik), the Lesser Himalaya, the Great Himalaya and the Tethys Himalaya or Tibet Himalaya (Himadri). The Indus–Tsangpo Suture Zone (ITSZ) is the northern boundary of the Indian plate. The boundary between the Tethys Himalaya and the Great Himalaya is marked by the Trans-Himadri fault. This fault was first identified as the Malari thrust (Valdiya 1979, Valdiya et al., 1984), and later redesignated as Trans-Himadri fault (Valdiya 1987, 1989). The Main Central thrust (MCT) is a major tectonic boundary between the Great Himalaya and the Lesser Himalaya with contrasting stratigraphy and tectonic features, whereas the Main Boundary thrust (MBT) separates the Lesser Himalaya from the Sub Himalaya with distinct geotectonics and formational regime. The Main Frontal thrust (MFT) separates the Sub Himalaya from the Indo-Genetic Plains. Its surface manifestations are visible at a few places (Fig. 1).

Table 1
The geographical co-ordinates and elevations of the recording stations.

SI no.	Station name (station code)	Latitude	Longitude	Height	Soil type
1	Ayanagar (Ayan)	28.482N	77.127E	220	Hard rock
2	Bahadurgarh (Bhgr)	28.688N	76.939E	214	Loamy and sandy soil
3	Bisrakh (Bis)	28.571N	77.439E	200	Alluvium soil
4	Dehradun (Ddi)	30.323N	78.056E	682	Hard rock
5	Dharmshala (Dhrm)	32.248N	76.307E	1995	Hard rock
6	Joshimath(Josi)	30.556N	79.558E	1889	Hard rock
7	Kalagarh(Kalg)	29.506N	78.754E	1814	Hard rock
8	Khetri(Khe)	28.074N	75.806E	320	Sandy soil
9	Kundal(Kudl)	28.144N	76.489E	227	Sandy soil
10	Kurukshetra(Kkr)	29.962N	76.821E	250	Sandy soil
11	Shimla(Smla)	31.128N	77.167E	2200	Hard rock
12	Sohna(Sona)	28.245N	77.063E	180	Sandy soil to loamy sandy soil

Many tectonic models have been proposed for the evolution of Himalaya (Seeber et al. 1981, Ni and Barazangi 1984, Yin and Harrison, 2000) with their own merits and demerits (Mishra 2014). The geodynamical implications of these models have not assured of common consensus with respect to seismogenesis. The Steady State Model postulates that the MCT and MBT converge with the plane of detachment, which marks the interface between the subducting Indian plate and overlying sedimentary wedge (Seeber et al. 1981). According to this model, the great Himalayan earthquakes have been related to the detachment surface. The Evolutionary model postulates that the zone of plate convergence progressively has been shifted towards south by the formation of intra-crustal thrusts. According to this model the MBT, the most active tectonic features and the seismicity concentrated in a 50 km wide zone between the surface trace of the MBT and the MCT (Ni and Barazangi 1984). The model suggests that the thrust zone propagates towards south along the detachment to the MBT and further south to the subsidiary blind thrusts making the MBT as most active thrust rooted in the detachment. The Main Central Thrust (MCT), the Main Boundary Thrust (MBT), and the Main Frontal Thrust (MFT) bear southward migration of main deformation front due to its young age and shallow depth. Nakata (1989) shows that some restricted parts of these thrusts exhibit neotectonic activity and active faulting on the surface.

It is intriguing to note that northern part of the Lesser Himalaya associated with the MCT zone that depict a belt of seismic activity (where moderate earthquakes ($5 \le M \le 5.9$) are frequent and are located mostly in the Garhwal and the Kumaon Himalaya (Khattri et al. 1989)), which falls in the present study area. Arita (1983) recognized another fault named as Munsiari fault or MCT-I, characterized by an abrupt change in lithology and metamorphic grade in the MCT shear zone below the MCT fault in the NW Himalaya and its adjoining parts. Another study demonstrated that the Lesser Himalayan Crystalline Nappes (LHCN) are formed either due to segments of the MCT hanging wall or thrust sheets carried by imbricates in the MCT footwall (Gansser, 1964). The duplex development in the MCT footwall has been related to the folding of the MCT and the LHCN (Burg et al. 1987) as shown in Fig. 1b.

Rigorous review on seismicity pattern of the NW Himalaya and its adjoining region made us understand that the seismicity in the NW Himalaya area generally follows the NW-SE trend and the clusters are mainly seen close to either the MCT or the MBT. A series of documentation on damaging earthquakes of the NW Himalaya and its adjoining region including the Great Kangra earthquake of 4th April 1905 (Mw 7.8) revealed that significant damages to property and death of people occurred in the region. Others earthquakes like, the Kullu earthquake of 28th February, 1906 (Mw 6.4), the Sultanpur earthquake of 11th May 1930 (M 6.0), the Chamba earthquake of 22th June 1945 (M 7.5), the Chamba-Udhampur earthquake of 12th September 1951 (M 6.0), the Lahual-Spiti earthquake of 17th June 1955 (M 6.0), the Kinnaur earthquake of 19th January 1975 (M 7.5), the Dharamshala earthquake of 26th April 1986 (M 5.0), the Uttarkashi earthquake of 1991 (M 6.8), the Chamoli earthquake of 1999 (M 6.6) and the Kashmir earthquake of 2005 (M 7.5) also caused severe losses to property and lives of people (Vandana et al., 2017, Vandana et al., 2016a, b). These observations suggest that the NW Himalaya and its adjoining region have complex seismotectonic settings with high potential of complex seismogenesis with varying degree of damages.

3. Data

In this study, we used 157 events as the best located events selected from 989 events ($2.2 \le Mw \le 4.9$) recorded during the period from January 2009–December 2017 by twelve digital seismographic stations (Table 1) network ascribed to National Centre for Seismology (NCS), Ministry of Earth Sciences, India. The epicentres of these 157 events are taken from ISC (International Seismological Centre) bulletin. In the present study, we relocated the 157 events with average combined root mean square (R.M.S.) error 0.49 s from 1.99 s. This indicates a significant reduction in R.M.S. value by 75.37%. These relocated 157 events are plotted on the tectonic map of the study area (Fig. 1b). Two types of sensors have been used for carrying out the study. Out of twelve stations, ten are short-period seismographs and two are of broad band seismographs. The data recorded with a sampling rate of 100 samples per second (sps) at Dehradun (Ddi), Dharmshala (Dhrm) and Shimla (Smla) stations, which limits the Nyquist frequency of 50 Hz, while at other stations the data recorded with a sampling rate of 50 samples per second (sps) at Ayanagar (AYAN), Bahadurgarh (BHGR), Bisrakh (BIS), Joshimath (JOSI), Kalagarh (KALG), Khetri (KHE), Kundal (KUDL), Kurukshetra (KKR) and Sohna (SONA) stations, which limits the Nyquist frequency of 25 Hz. We considered waveforms having signal to noise ratios (SNR) above 3 in our analysis. A total of 777 velocity time histories have been used for the analysis in which one earthquake is recorded minimally by 3 seismographic stations and maximally by 11 seismographic stations as shown in Appendix 1.

4. Methodology and data analysis

Our approach is based on the application of Brune model (Brune 1970) for making estimates of source parameters, which has proven track record of its applicability in the region of diverse tectonic settings, elsewhere in the world (Hiramatsu et al. 2002, Kumar et al. 2006, Kumar et al. 2008, Kumar et al. 2015, Vandana et al., 2017, Sairam et al., 2018). In this model, the single spectrum fitting followed by estimating average over the stations were performed. Several terms of an elastic attenuation model, such as high frequency content, Kappa and f_{max} have been described for understanding their bearing on geodynamical aspects of the NW-Himalaya and its adjoining region. In the present study, the best located events having precise magnitudes that ensured the nullification of the effect of trade-off among different estimated source parameters. According to Brune's model the displacement and acceleration spectra of an earthquake can be written as:

$$\mathrm{D(R,f)} = \frac{\mathrm{C}\Omega_0}{1+\left(\frac{\mathrm{f}}{\mathrm{f_c}}\right)^2} \text{ and } A(R,f) = \frac{C\,(2\pi \mathrm{f})^2\Omega_0}{1+\left(\frac{f}{f_c}\right)^2} \tag{1}$$

where D(R, f) and A(R, f) represent the amplitudes of displacement and acceleration spectra, and f_c, Ω_0, & C signify corner frequency, low frequency spectral level, and a constant scaling term, respectively. To model the decay of acceleration spectrum at high frequencies beyond $f_{max,}$ two functions has been adopted. The first function $P_1(f)$ represents a high-cut filter which is expressed as given below (Wen and Chen 2012),

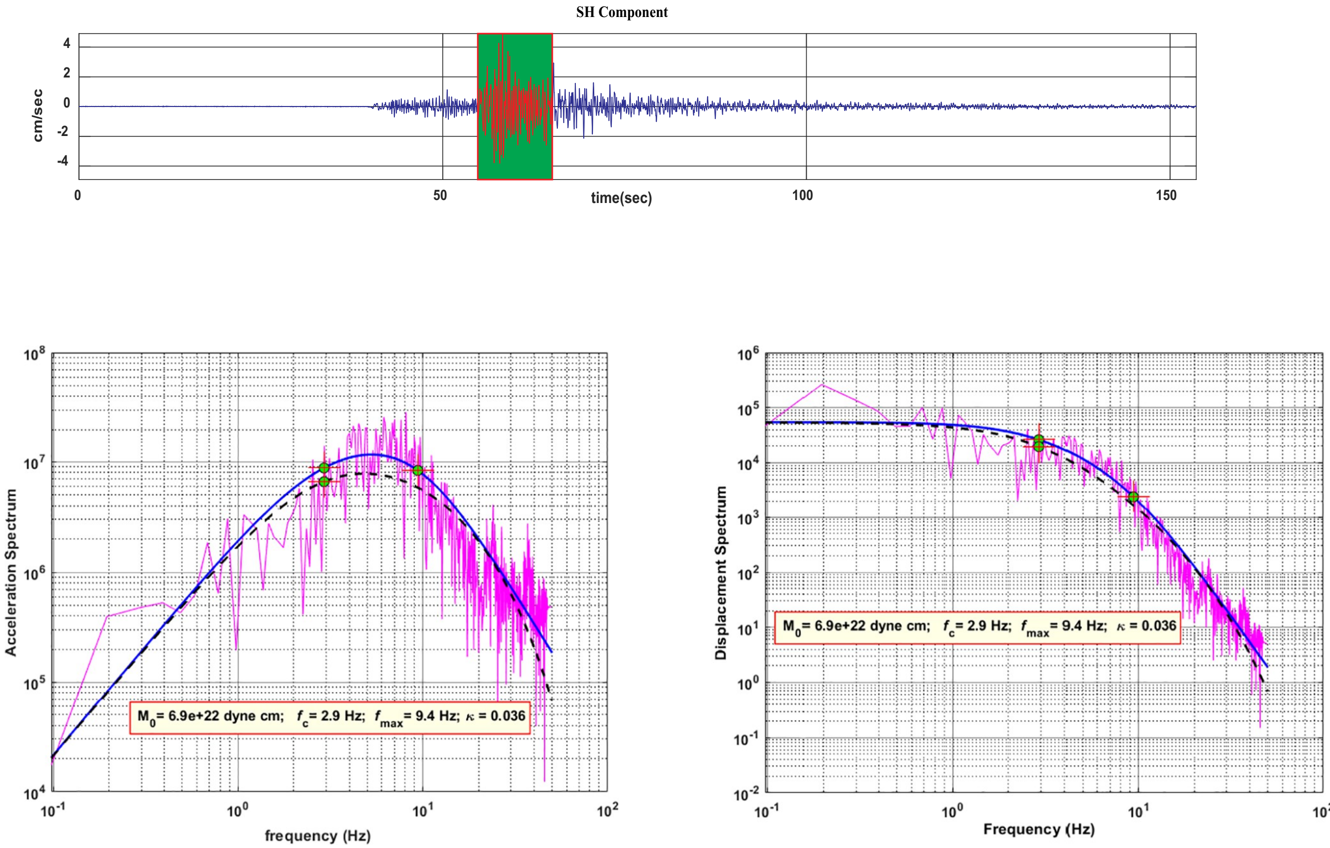

Fig. 2. A sample record showing an example of SH component of time history of earthquake recorded at DDI (Dehradoon) on broadband seismometer (top). The acceleration (bottom left) and displacement (bottom right) spectra along with fitted source model.

$$P_1(f) = \frac{1}{1 + \left(\frac{f}{f_{max}}\right)^p} \quad (2)$$

where p is a non-negative real number. This function has been used to estimate f_{max}, and slope of the spectrum above f_{max}. The second function has the exponential form:

$$P_2(f) = e^{-\pi f \kappa}, \quad (2a)$$

where, in the Eq.(2a), the parameter Kappa (κ) is used to model high frequency attenuation (Anderson and Hough 1984). Both these expressions has been incorporated in the software EQK_SRC_PARA (Kumar, 2011), and the modified software was adopted to estimate the source parameters. From the acceleration spectrum, the spectral parameters which include: Ω_0, fc, f_{max} and spectrum level at an intermediate frequency level are manually picked-up. Kumar et al. (2012a, b) have described the method and the steps used in the software in detail. The p and κ parameters have been estimated separately.

From the spectral parameters $\Omega_0$and fc, the source parameters, viz., M_o, r and $\Delta\sigma$ have been estimated using the following expressions given by Brune (1970):

$$M_o = \frac{4\pi\rho\beta^3 R\Omega_0}{R_{\theta\varphi}.\ S_a}$$

$$r = \frac{2.34\beta}{2\pi f_c}$$

$$\Delta\sigma = \frac{7M_o}{16r^3}$$

where ρ, β, R, $R_{\theta\phi}$ and S_a represent the average density, shear wave velocity, hypocentral distance, the average S-wave radiation pattern, and free surface amplification, respectively. For the NW Himalaya and its adjoining region the value of "ρ" and "β" are taken as 2.67 g/cm^3 and 3.4 km/s, respectively (Kumar et al., 2014a, b). The values of $R_{\theta\phi}$ and S_a are assumed to be 0.63 and 2, respectively. The moment magnitudes (M_w) have been estimated from M_o using the equation (Hanks and Kanamori 1979):

$$M_w = \frac{2}{3}\log(M_o) - 10.7$$

The average values of source parameters, f_{max} and κ has been estimated from the following expression (Archetula et al., 1982)

$$x_{avg} = anti\log\left(\frac{1}{N}\sum_{i=1}^{N}\log x_i\right) \quad (3)$$

where, N signifies the number of stations on which an event gets recorded. The standard deviations (SD) of the source parameters ($x = M_w$, M_o, Δσ, and r) have been estimated from the variance of the individual logarithmic values adopting the following equation:

$$SD(\log x_{avg}) = \left[\frac{1}{N-1}\sum_{i=1}^{N}(\log x_i - \log x_{avg})^2\right]^{1/2} \quad (4)$$

5. Estimation of spectral and source parameters

In order to resolve different parameters for mitigating mutual trade-off among source parameters, we generated corrected source spectrum to assess spectral parameters (viz. Ω_0, f_c, f_{max} and Kappa) and source parameters of each event, which has been estimated from SH component of the ground motion, using the tool which has already been applied for other Indian regions (A. Kumar et al., 2006; D. Kumar et al., 2006, Kumar et al. 2008, Kumar et al., 2012a, b, Kumar et al. 2015, Vandana et al., 2017). The digital time series of events have been corrected for baseline as well as for instrument response. In order to analyse source spectra, the observed spectra were corrected for path effect using the frequency dependent attenuation relation $126{*}f^{1.12}$ estimated for the NW Himalaya and its adjoining region (Vandana and Mishra, 2018). A typical example of the time series of earthquakes along with the fitting of Brune's model obtained from the estimated source parameters to the observed spectra at Dehradun station (DDI) is shown in Fig. 2. The relocated hypocentral parameters of 157 events are listed in Appendix 1. Source parameters, namely, seismic moments, source radii and stress drops for these events have been estimated and are shown in Appendix 2 with corresponding standard deviation (S. D.) values. Our estimates showed that S.D. of seismic moment (M_o), moment magnitude (Mw), radius (r) and stress drop ($\Delta\sigma$) are varying from 0.01 to 2.47, 0.01 to 0.51, 0.01 to 0.75, and 0.01 to 1.98, respectively with their corresponding average variation of 0.78, 0.07, 0.24, and 0.68. It is worth to mention that Brune source model works effectively for the stress variation either lesser or equal to 100 bars. Additionally, the approach that we used in the present study is found to have poor fit for source spectra for events of $M \geq 5$.

6. Results and discussion

Fig. 3 shows the variation between the seismic moment and source radii at constant stress drop with corresponding moment magnitude lies ($2.2 \leq M_w \leq 4.9$). The source dimensions in terms of radius of the circular fault varied from 148 m to 975 m. It is observed that about 83% events have stress drop between 0.1 bar and 10 bar whilst 16% events have stress drop between 10 bar and 100 bar. The events which correspond to stress drop varying from 0.1 bar to 10 bar show a significant variation in a stress drop with the seismic moment varying from 2.64×10^{19} dyne-cm to 2.32×10^{23} dyne-cm. It has been observed that the source radii increased linearly with seismic moments, which is in unison to the general seismological phenomenon. However, this increment is not very evident for events having stress drop changed from 10 bar to 100 bar due to large scatter in data. It has been found that the average stress drop for the NW Himalaya for earthquake ($2.2 \leq Mw \leq 4.9$) is about 27 bars. Kumar et al. (2016) found the average stress drop for the NW Himalaya of about 40 bar. Moreover, Kanamori and Anderson (1975) found the average stress drop of 60 bars from the empirical studies for moderate to large earthquakes. Based on these observations, we can infer that variability in stress drop ($\Delta\sigma$) for given seismic moment (M_o) is attributed to different but intricate seismogenic sources of varying strengths that may have bearing to the nature of structural heterogeneities (strong, weak and compliant) of source rocks from where earthquakes get originated (Mishra et al. 2005a, 2005b; Mishra et al. 2008).

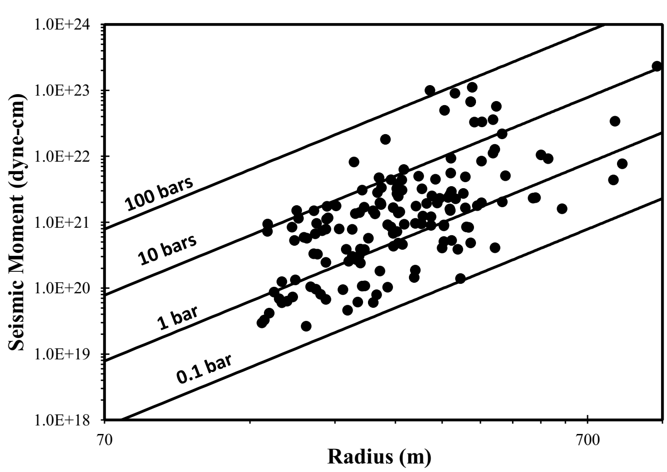

Fig. 3. A plot between source radius and seismic moment.

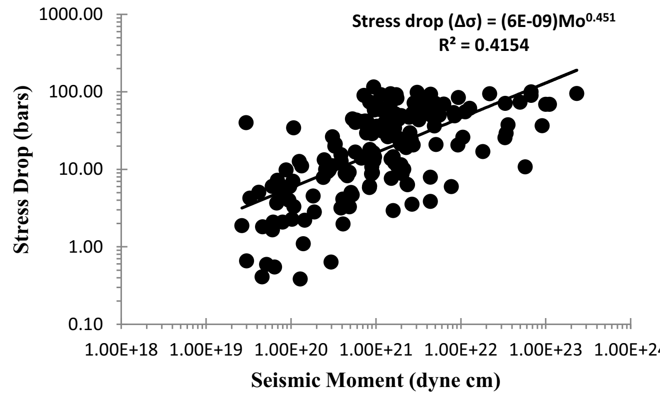

Fig. 4. A plot between seismic moment and stress drop.

6.1. Implications of Seismic moment and stress drop

Fig. 4 shows the variability in stress drop for the given seismic moment which could be attributed to different seismic sources of varying strengths. It has been observed that the data points are scattered from 1×10^{19} dyne-cm to 1×10^{21} dyne-cm without variation in stress drop. Beyond 1×10^{21} dyne-cm the stress drop is almost constant with respect to seismic moment. This analysis showed the presence of self-similarity among the earthquakes sources for the given magnitude range for which the rupture processes of earthquakes also maintained self similarity for the NW Himalaya and its adjoining region. Analysis of 12-earthquakes by Kumar et al. (2008) showed the self-similarity among the moderate and large earthquakes of the NW Himalaya, which, however based on analyses of scanty data. Recently, Kumar et al. (2016) also showed the existence of self-similar nature among the moderate size earthquakes for the NW Himalaya by analysing strong ground accelerograms (SMA).

Self similarity of earthquake genesis has been studied by different researchers for different regions to understand the exact physics. Abercrombie's (1995) showed the constant stress drop scaling for the earthquakes for varying magnitude ($-1 < M < 5$), that occurred in Cajon Pass borehole, Southern California. Bindi et al. (2001) found the self-similar nature among the Umbria-Marche (Italy) seismic sequences. Cantore et al. (2011) also showed the self-similarity among the earthquakes of Southern Apennines, Italy. Similarly, Prejan and Ellsworth (2001) found the constant static stress drop over entire magnitude range for the Long Valley Caldera, Eastern California. Based on these observations, our results also bear a good correspondence to the nature of self-similarity studies made by different researchers, elsewhere in the world, and we found that seismic moment of different earthquakes of varying strengths bear a self similarity relationship with stress drop, which in turn controls the degree and extent of seismic potential of the region.

6.2. Implication of Stress drop and depth variability

Fig. 5 shows that the stress drop increases systematically with depths of earthquakes that corroborate shear stress in the brittle crust demonstrating a linear increase of stress drop with depth (Mcgarr 1980). Additionally, crustal strength of source zones also increases linearly with depths (Sibson 1974). We observed that at higher stress drop, the depth variability is very large, signifying different geological seismic sources. It suggests that stress drop ($\Delta\sigma$) of events have good bearing on source depths, indicating the shear stress regime in the brittle crust may control the extent of stress drop at varying source depths. Significant changes of stress drop showing higher value with very large variability in depth, which in turn suggests the presence of intricate subsurface seismogenic sources beneath the NW Himalaya and its adjoining region (Fig. 5). It is so because the nature of seismogenic

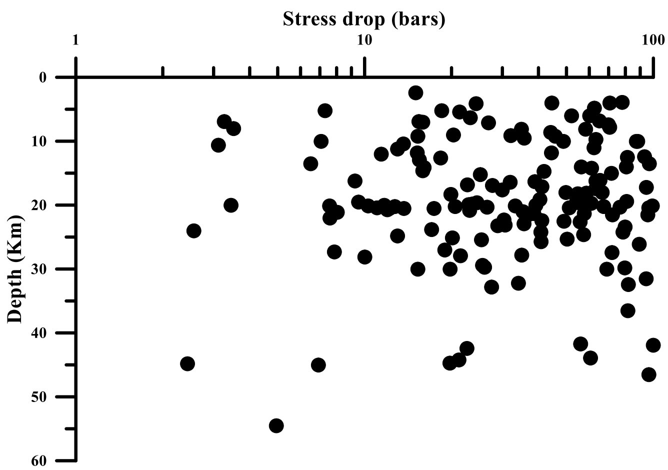

Fig. 5. A plot between stress drop and focal depth.

sources controls the extent of stress accumulation and strain energy release (Mishra and Zhao 2003; Mishra et al. 2008).

6.3. Implication of Seismic moment versus corner frequency

As mentioned above, investigations of self-similar behaviour of earthquakes were made by many researchers in the past (Hiramatsu et al. 2002; Kumar et al. 2006; Kumar et al. 2008; Kumar et al. 2013b; Kumar et al. 2015). Aki (1967) proposed that small and large earthquakes are geometrically similar and scaling relations are defined by interdependence of various parameters, such as magnitude, seismic moment, fault dimension, stress drop, corner frequency, and seismic energy. Alternately, Kanamori and Anderson (1975) developed a theoretical basis for the scaling relations of source parameters, which also been used by Kumar et al. (2013b). One of the greatest implications of this scaling law is almost constant stress drop for majority of earthquakes that can have applicability to assess geodynamical implications. However, scaling relations may vary from region to region because of the variation of stress drop is associated with nature and complexity of seismogenic source zones.

The scaling relation between the seismic moment, M_o, and corner frequency, f_c, has the following general form proposed by Aki (1967):

$$Mo \propto f_c^{-3}$$

Above relation implies that the static stress drop, Δσ, is constant and independent of earthquake size. In this study we also attempted to derive a scaling relationship between seismic moment, M_0, and corner frequency, f_c using a total of 157 events (Fig. 6), which is found to be as:

$$M_0 = 8 \times 10^{22} f_c^{-2.89}$$

The deviation from above relation has been expressed by Izutani and Kanamori (2001) and Kanamori and Rivera (2004) as:

$$Mo \sim f_c^{-3+\varepsilon}$$

where, ε is a constant < 1 and ε reflects that either static stress drop or rupture velocity or both depend on the earthquake size (Kanamori and Rivera 2004; Venkataraman et al. 2006; Kumar et al. 2013b). Based on these considerations, we estimated ε-value with reference to $f_c^{-3+\varepsilon} = f_c^{-2.89}$ that resulted in ε = 0.11 as the extent of static stress drop or rupture velocity. we interpreted that the dependency of source size is either on stress drop or rupture velocity or both. As mentioned above, seismic moment (M_0) and corner frequency (f_c) are in good unison to the Garhwal and the Kumaon Himalaya (Kumar, 2011), indicating that the NW Himalaya and its adjoining source zone have similar source characteristics with analogous seismogenic potential to that of the Garhwal and the Kumaon Himalaya region.

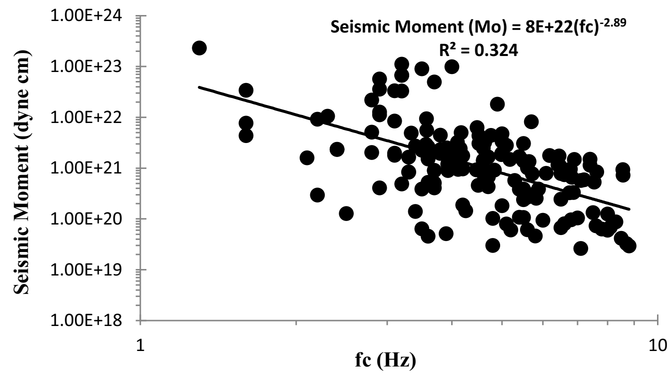

Fig. 6. A plot between seismic moment and corner frequency.

We also analysed our data in terms of f_{max} to get insight into the source characterisation of our study region in terms of variability of seismic moment with f_{max} (Fig. 7-l). It is a matter of detailed seismological analysis to understand whether the f_{max} observed in the acceleration spectrum of an earthquake reflects the source characteristics or it is related to attenuation of seismic wave due to subsurface geological characteristics beneath the recording site (Hanks 1982, Papageorgia and Aki, 1983a, b, Anderson and Hough 1984, Anderson 1986, 1991, Kumar et al. 2013b). Fig. 7 shows the variation of f_c and f_{max} with seismic moment for each site having relationship with seismic source. Although the data shows large scatter but assuming almost similar decreasing trend for both f_c and f_{max} with increasing seismic moment or source size. Hence, it can be concluded that f_{max} has similar dependence as f_c on seismic source. The plots shown in Fig. 7e, h, i, j and k indicate a large scatter having almost parallel trends for both f_c and f_{max} with increasing seismic moment. Thus, these observations suggest that f_{max} has similar behaviour as f_c with seismic moment on each site, which in turn supports the fact that both f_c and f_{max} are due to source processes. Similar results have been reported by Tsai and Chen (2000) and they showed the high-cut process (f_{max}) is controlled by both the site and source effects. They also inferred that distance is the least significant parameter in controlling the f_{max}. Studies using local events showed that the dependence of f_{max} on source effect for the Kameng region of the Arunachal Lesser Himalaya (Kumar et al., 2013a, b), the Lower Siang region of Arunachal Lesser Himalaya (Kumar et al. 2015), and the Bilaspur region of the Himachal Lesser Himalaya (Kumar et al., 2013a, b, Paidi et al. 2015, Vandana et al., 2017) that corroborate to our present interpretation of f_{max} for the NW Himalaya and its adjoining region.

6.4. Implication of Kappa (κ)

In order to understand the nature and extent of the structural heterogeneity of sites, we estimated Kappa (κ) using our high quality data. Figs. 8–10 show the variation of Kappa with epicentral distance, number of events, and their magnitudes, respectively. At BHGR, BIS, DHRM, AYAN, KALG, KHE, KUDL, KKR, DDI, JOSI and SONA sites, the Kappa values range with distinct variability in increment, such as 0.02–0.04, 0.02–0.03, 0.02–0.04, 0.02, 0.02–0.03, 0.02–0.06, 0.02–0.08, 0.01–0.07, 0.02–0.03, 0.01–0.04 and 0.02–0.08 s, respectively. Our estimates of Kappa and its variability with reference to epicentral distance (0–600 km) revealed that majority of the best located events recorded at varying epicentral distances occurred in a source zone with values varied as 0.01 ≤ κ ≤ 0.08 s. However, it is pertinent to note that epicentral distance has no role in influencing the number of events (Fig. 8). It has been observed that with increase of Kappa (0.01 ≤ κ ≤ 0.03 s), the number of the events gets reduced from 298 to 188 as shown in Fig. 9. The minimum number of events (50) is found to fall in a source zone, which is associated with higher Kappa

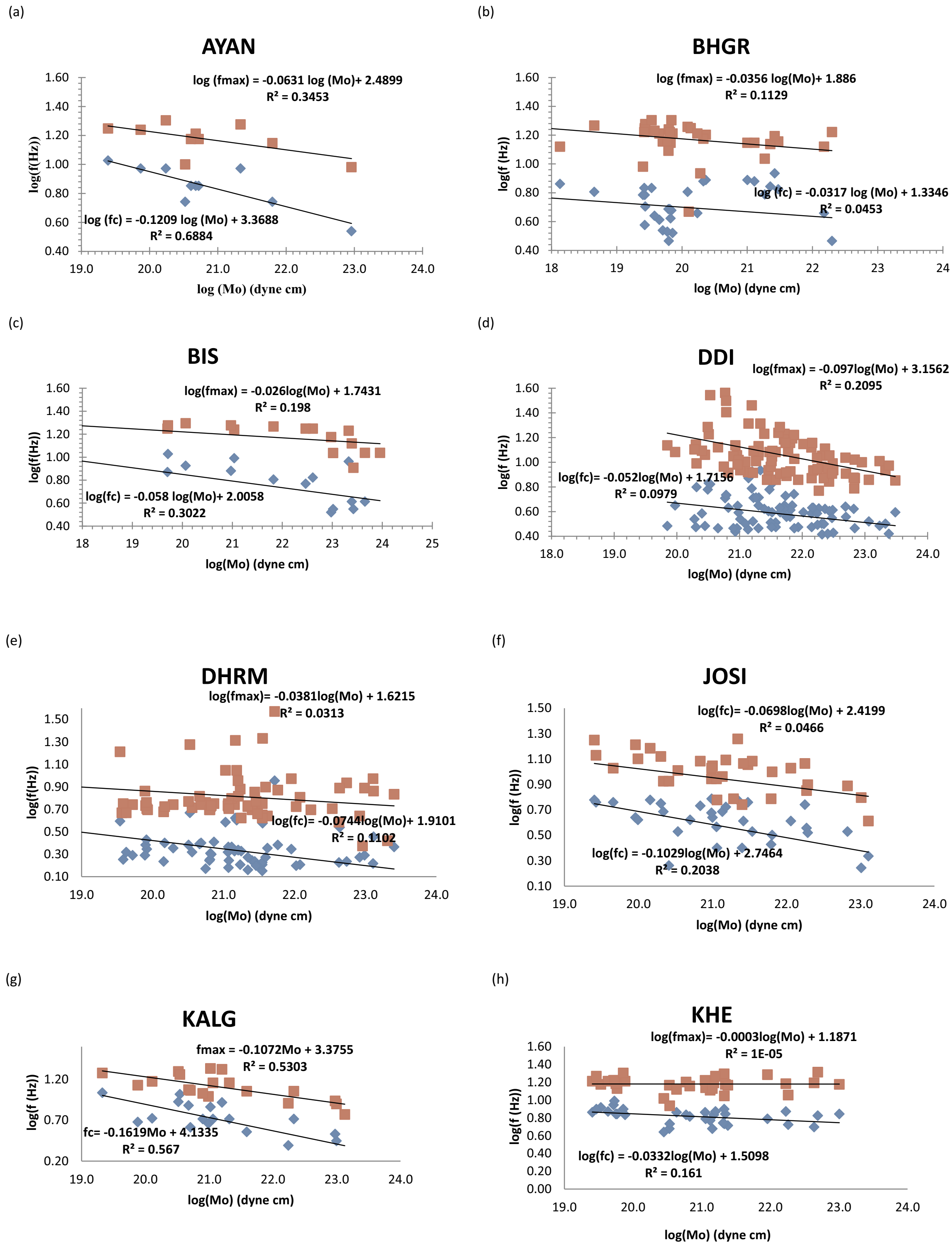

Fig. 7. a–l A plot showing variation of f_c and f_{max} with seismic moment for twelve sites.

values varying from 0.06 s to 0.08 s. We may infer that Kappa is an indicator of geomechanical strength for the seismogenic layers beneath the NW Himalaya and its adjoining region, which suggest that more number of the events with the lowest Kappa values may correspond to the source zone associated with weak structural heterogeneity, whilst the minimum number of the events associated with relatively higher values of Kappa is suggestive of comparatively a strong structural heterogeneity of the source zone. This observation is supported by the fact that the structural heterogeneity dictates the propensity of occurrences of events (Mishra 2012, Lei et al. 2012, Lei et al. 2012, Singh et al., 2012, Singh et al., 2013, Mishra, 2013). In order to ascertain the strength of the events and their interrelationship with Kappa, we attempted to see the variability between the magnitude of the best located events and Kappa value, which shed a enough light on the fact that the lower number of events correspond to the higher strength of the source zone from where events of relatively higher magnitudes occurred, and similarly higher number of events of relatively lesser magnitudes occurred in the weaker source zones associated with

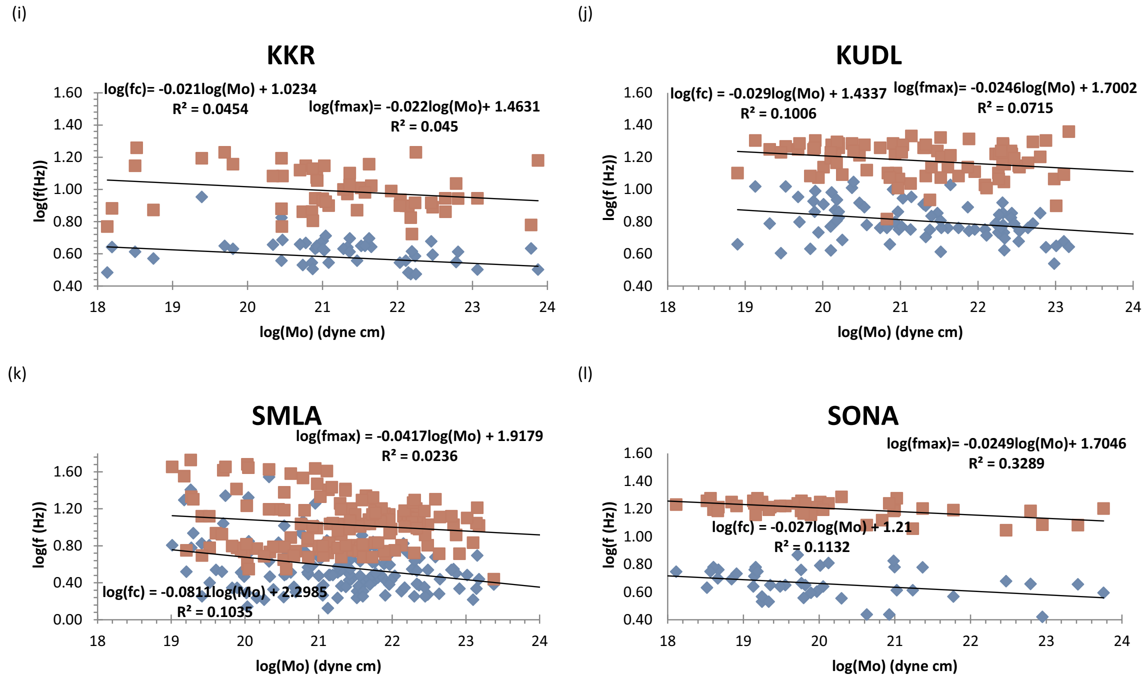

Fig. 7. (*continued*)

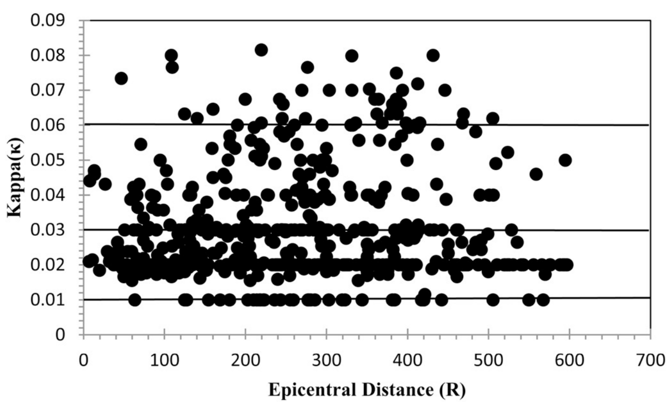

Fig. 8. A plot showing variation of kappa with epicentral distance.

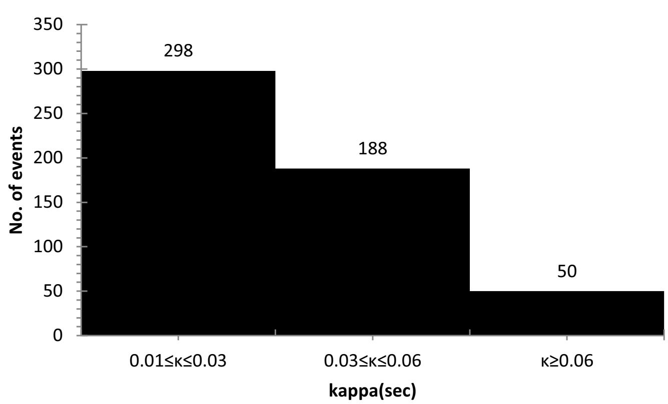

Fig. 9. A plot of Kappa with respect to number of events.

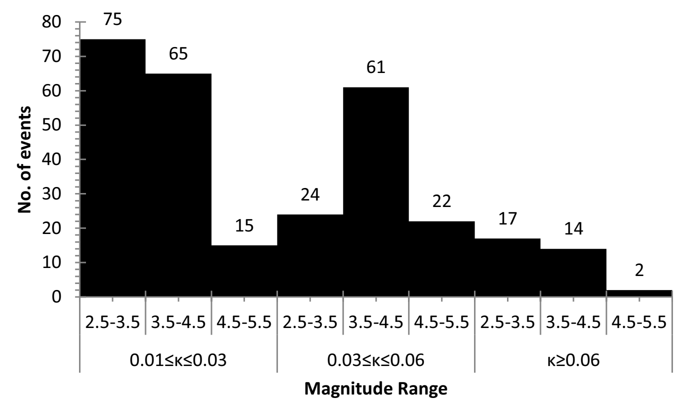

Fig. 10. A plot showing magnitude range corresponding to Kappa values with respect to number of events.

comparatively lower Kappa values as shown in Fig. 10. It is worth to mention that different sites in the Garhwal and Kumaon Himalaya showed estimates of Kappa from strong motion records varied between 0.023 s and 0.07 s with its average value of 0.044 s (Sharma, 2014). It appears that for the NW Himalaya and its adjoining region the average value of Kappa lies between 0.01 s and 0.08 s., which is comparable with the Garhwal and Kumaon Himalaya. We conclude that occurrences of majority of earthquakes of micro-to-moderate strengths ($2.5 \le M \le 5.0$) at different depths found associated with Kappa values that varied between 0.01 s and 0.08 s and this observation supports the existence of weaker heterogeneity beneath the source zones of the NW Himalaya and its adjoining region that may control the extent of the background seismicity. Depending upon the geology and soil profile beneath the seismographic stations (Table 1), it is evident that hard rock geology and soft rock geology have strong bearing on variability in values of kappa.

It is pertinent to mention that the Kachchh region of Western India showed variability in Kappa estimates between 0.025 and 0.03 s (Mandal and Johnston, 2006), whilst various parts of the world demonstrated significant changes in Kappa values that encompass a broad range from 0.003 s to 0.08 s (Chandler et al., 2006a, b). Purvance and Anderson (2003) estimated Kappa considering earthquakes over a wide range of magnitudes of earthquakes ($3.0 \le M \le 8.0$) and they found that the κ is primarily controlled by source characteristics. However, modeling of spectral amplitudes at high frequencies (> 15 Hz) as a product of Brune spectrum and exponentially decaying function suggested that the significant variation is attenuation properties of the medium over a small distance range of tens of meters may affect κ values (Tusa et al. 2012). We can infer from estimates of different source parameters for varying strength of events at different depths that earthquake sources are associated with varying seismogenic potential beneath the NW Himalaya and its adjoining region because of variation in structural heterogeneities may influence source characteristics of the earthquake, suggesting intricate geodynamical set-up beneath the NW Himalaya and its adjoining region.

7. Conclusions

In this study, a comprehensive study on source characterisation of the NW Himalaya and its adjoining region is made by analysing high quality data recorded by a well defined seismographic network with adequate sampling rate and Nyquist frequency that provided scope of analysing the corrected source spectrum and the values of spectral parameters, such as, low frequency spectral level (Ω_0), corner frequency (f_c), high-cut frequency (f_{max}), and Kappa (κ), different source parameters seismic moments (M_o), source radii (r), stress drops ($\Delta\sigma$) and moment magnitudes (M_w) of the events. There is a systematic variation of source dimension in terms of the source radii of the circular fault with distinct changes in the static stress drops and seismic moment (M_o). We infer that variability in stress drop ($\Delta\sigma$) for seismic moment (M_o) is attributed to different seismic sources of varying strengths associated with varying structural heterogeneities of the source zones. Additionally, a scaling relationship between seismic moment (M_0) and corner frequency (f_c) for the region is found as: $(M_0) = 8 \times 10^{22} f_c^{-2.89}$, which is in good unison to the Garhwal and the Kumaon Himalaya, indicating that the NW Himalaya and its adjoining source zones may have similar source characteristics with analogous seismogenic potential to that of the Garhwal and the Kumaon Himalayan region. One of the greatest implications of this Scaling law is that almost constant stress drop for a large range of earthquakes has been observed in the present study. However, scaling relations may vary from region to region because of the variation of stress drop due to nature of seismogenic source zones. We propose to develop a regional Scaling law for understanding the comprehensive behaviour of the sub-surface seismogenic crust and its attenuative behaviours beneath the NW Himalaya and its adjoining region. Stress drop ($\Delta\sigma$) of the events have strong bearing on source depths, suggesting the shear stress regime in the brittle crust, which has linear relationship with $\Delta\sigma$ and source depth. It is intriguing to observe that significant changes of stress drop ($\Delta\sigma$) of higher value with very large variability at depths are suggestive for the presence of intricate subsurface seismogenic sources beneath the NW Himalaya and its adjoining region. Occurrences of majority of earthquakes of micro-to-moderate strengths ($2.5 \le M \le 5.0$) at different depths found associated with Kappa values that also supported the prevalence of weaker heterogeneity beneath the source zones of the NW Himalaya and its adjoining region which controls the nature and extent of background seismicity. Our interpretation of near surface attenuation factor (κ) suggests that the nature and extent of structural heterogeneity and seismogenesis are closely and linearly related to each other, which in turn demonstrates that higher kappa (κ) is associated with the strong structural heterogeneity where lesser number of moderate to strong earthquakes may occur and reverse is also true.

Estimates of different source parameters and their interrelationship with varying strength of events at varying depth clearly suggest that NW Himalaya and its adjoining region have intricate geodynamical set-up which has been dictated by structural heterogeneities of varying source characteristics, which in turn influencing the propensity of the background seismicity and controls the seismogenic potentials of the region.

Acknowledgements

The authors are thankful to the Secretary, Ministry of Earth Sciences (MoES), Government of India for support and encouragement for conducting research activity with seismological data recorded at National Centre for Seismology (NCS), Ministry of Earth Sciences, New Delhi. Authors are grateful to the Director, NCS, MoES, New Delhi for his consistent support, motivation and constructive discussion for generating plausible outcomes out of this study. Stimulating discussion with colleagues at NCS – MoES, like G. Suresh, J.L. Gautam, Babita Sharma, Sunil Rohilla, and Varun Sharma is gratefully acknowledged. Special thanks to Vikas Kumar, NCS-MoES for his help in improving plots and figures for the revised version of the manuscript. A special vote of thanks to Dr. Arjun Kumar, Arni University, Kathgarh (Indora) for his meticulous lesson on computational aspect of the source code used in this study.

Appendix 1. Showing the relocated hypocenter parameters of 157 events that occurred beneath the NW Himalaya and its adjoining region

Si no.	Date	Time	Latitude	Longitude	Depth	Magnitude (Mw)	Number of stations recorded the earthquake
1	08-10-2009	17:23:56	28.990	77.082	22	2.6	7
2	10-10-2009	09:12:30	31.092	74.529	16	3.5	5
3	20-10-2009	23:44:07	30.669	77.782	22	3.4	6
4	27-10-2009	20:16:13	30.275	76.310	2	3.0	3
5	08-12-2009	07:05:15	30.557	79.924	26	3.8	3
6	05-01-2010	15:04:35	30.644	79.609	10	3.6	7
7	11-01-2010	05:15:26	29.505	79.140	23	4.0	4
8	13-01-2010	10:18:03	28.687	77.129	20	2.9	3
9	05-03-2010	05:15:49	29.217	77.238	16	2.7	3
10	16-03-2010	05:23:01	29.225	77.295	20	2.8	9
11	07-04-2010	07:05:49	28.059	76.654	47	3.4	5
12	22-05-2010	17:34:10	28.01	77.211	10	2.5	3
13	26-01-2011	03:06:43	29.083	77.423	42	3.2	4
14	06-02-2011	16:16:53	31.416	76.124	15	3.6	3
15	21-03-2011	01:07:01	29.915	77.00	20	3.9	3
16	25-03-2011	07:19:25	29.089	77.007	21	2.8	3
17	04-04-2011	11:31:32	28.052	77.801	62	4.9	11
18	28-04-2011	09:52:57	32.660	76.350	28	4.2	3
19	04-05-2011	20:57:09	30.763	74.502	37	4.6	10
20	29-05-2011	00:05:39	28.279	76.396	6	3.5	7
21	07-06-2011	09:08:29	31.432	76.31	18	4.4	9
22	20-06-2011	06:27:13	29.985	79.336	10	4.8	9

23	02-07-2011	11:01:09	29.546	79.137	45	2.5	4
24	03-07-2011	03:49:30	31.040	76.090	20	3.5	6
25	04-07-2011	09:44:03	30.550	79.387	17	3.4	6
26	23-08-2011	20:14:03	28.821	76.788	8	2.5	5
27	07-09-2011	00:55:33	30.907	76.527	5	3.7	5
28	07-09-2011	17:58:17	28.762	77.144	23	3.8	4
29	26-09-2011	21:17:10	30.709	78.961	55	2.7	8
30	12-10-2011	10:27:25	28.158	75.937	13	3.5	5
31	07-01-2012	15:31:03	29.700	78.551	24	2.7	10
32	13-01-2012	01:26:11	30.914	76.511	8	3.6	10
33	22-01-2012	04:38:20	28.944	76.725	10	3.0	8
34	10-04-2012	00:52:16	31.065	76.924	16	3.8	6
35	22-04-2012	05:51:54	28.875	74.251	20	2.8	4
36	17-05-2012	13:39:18	28.924	76.725	13	3.4	5
37	13-06-2012	03:16:03	28.866	76.710	25	2.8	4
38	22-06-2012	02:44:44	29.176	76.944	10	3.5	7
39	22-06-2012	04:38:46	29.153	76.956	20	3.4	4
40	17-07-2012	10:26:50	30.910	73.684	21	3.9	4
41	02-09-2012	18:52:51	28.839	76.537	14	2.5	3
42	16-09-2012	19:29:04	28.973	77.523	20	3.3	6
43	02-10-2012	08:34:49	32.143	76.045	24	4.6	5
44	08-10-2012	17:46:21	31.850	78.470	9	4.8	5
45	11-10-2012	13:21:01	31.790	77.341	45	3.4	4
46	30-10-2012	17:22:35	28.006	71.969	30	3.3	3
47	06-11-2012	12:21:08	32.382	76.048	14	3.9	3
48	11-11-2012	20:23:08	32.343	76.102	25	3.9	7
49	15-11-2012	06:46:05	28.5	76.703	28	3.0	3
50	19-11-2012	06:25:19	28.891	76.419	10	3.7	9
51	24-11-2012	20:22:57	30.660	74.485	21	4.1	4
52	25-11-2012	16:04:41	33.701	76.10	20	3.9	3
53	27-11-2012	12:15:13	30.675	78.374	42	4.3	7
54	03-12-2012	04:34:43	31.039	74.494	21	3.8	4
55	02-01-2013	10:55:51	31.660	77.470	5	3.5	3
56	02-01-2013	17:42:13	29.885	77.023	20	4.7	4
57	10-01-2013	15:16:08	30.8	78.302	11	4.0	5
58	29-01-2013	19:42:56	29.323	76.613	20	3.7	4
59	06-02-2013	08:22:45	28.776	76.704	30	3.0	5
60	07-02-2013	01:08:37	29.646	76.811	44	3.8	3
61	08-02-2013	23:02:26	30.021	72.477	20	3.6	4
62	17-02-2013	16:27:08	30.913	78.413	7	2.8	5
63	25-02-2013	02:28:26	30.590	78.042	33	3.6	4
64	26-03-2013	21:06:02	29.620	79.940	45	2.9	4
65	04-04-2013	17:38:47	33.091	71.944	30	3.9	3
66	06-04-2013	22:29:28	30.549	79.041	22	3.6	6
67	25-04-2013	14:38:35	29.568	77.811	24	3.7	3
68	27-04-2013	07:41:38	29.217	78.605	20	3.0	7
69	04-06-2013	17:34:38	32.593	76.030	30	4.9	7
70	05-06-2013	22:03:54	32.742	76.175	19	4.1	4
71	29-06-2013	15:22:22	28.704	76.792	11	2.6	4
72	09-07-2013	13:48:58	32.581	79.179	14	5.0	5
73	13-07-2013	17:49:22	31.565	75.186	6	4.3	6
74	15-07-2013	17:49:06	31.998	75.506	7	3.7	4
75	18-07-2013	12:55:19	28.430	77.522	21	3.0	5
76	22-07-2013	09:07:14	32.304	74.792	12	3.8	5
77	05-08-2013	07:26:56	28.903	70.280	14	3.9	4
78	05-09-2013	11:29:23	28.873	74.273	20	3.1	3
79	23-09-2013	13:26:07	26.274	79.040	16	4.5	3
80	11-10-2013	18:05:31	28.803	76.932	20	3.3	5
81	26-10-2013	00:04:54	32.208	75.431	42	4.5	5
82	26-10-2013	00:44:49	28.730	76.597	11	3.0	3
83	21-02-2014	07:25:58	29.767	75.917	20	3.5	5
84	19-05-2014	21:53:33	31.891	77.133	20	4.0	3
85	22-10-2014	10:55:22	28.900	77.310	20	2.9	4
86	09-01-2015	21:58:43	30.846	78.869	6	2.8	3
87	24-01-2015	19:09:39	30.224	77.028	15	2.7	7
88	02-03-2015	03:33:30	32.869	77.001	18	2.6	11
89	23-03-2015	11:53:24	30.525	79.603	7	3.4	10
90	29-03-2015	06:49:29	32.769	77.183	25	3.6	4
91	29-03-2015	20:40:14	33.777	77.363	23	3.7	5
92	23-04-2015	22:48:28	33.208	77.059	18	3.4	3
93	08-05-2015	05:08:31	29.384	77.115	9	3.3	6
94	23-05-2015	11:53:59	30.716	79.094	18	3.4	4
95	02-06-2015	06:34:25	29.276	76.907	10	3.6	4
96	28-06-2015	07:52:29	32.251	74.974	15	3.6	3
97	12-07-2015	13:44:57	28.867	76.174	15	2.7	9
98	18-07-2015	23:48:10	29.415	77.779	20	4.7	7
99	06-08-2015	21:44:09	30.683	78.549	7	3.1	7
100	19-08-2015	19:18:13	31.270	76.702	7	3.8	8
101	25-08-2015	08:41:02	30.643	77.354	17	3.6	6
102	03-09-2015	07:59:23	30.816	79.782	21	3.5	4

103	03-09-2015	17:58:00	32.098	76.011	14	4.2	3
104	15-09-2015	22:38:19	32.01	76.01	21	4.5	3
105	06-10-2015	04:17:44	29.022	76.992	8	3.0	5
106	08-10-2015	01:04:17	31.256	76.690	5	4.2	3
107	09-10-2015	20:29:59	30.700	78.322	9	3.3	4
108	02-11-2015	17:35:01	29.268	76.688	18	3.2	4
109	05-11-2015	16:26:58	31.007	74.510	19	3.5	5
110	06-12-2015	12:35:05	28.516	76.850	21	3.4	4
111	29-12-2015	00:07:00	32.106	75.141	22	4.7	5
112	29-12-2015	15:50:21	29.207	76.395	21	3.3	4
113	28-01-2016	22:47:22	32.125	76.296	27	3.7	4
114	30-01-2016	09:39:32	28.423	76.774	13	3.1	3
115	09-02-2016	15:13:47	30.954	74.963	22	4.2	4
116	21-03-2016	00:18:54	30.611	79.511	17	2.6	6
117	23-05-2016	01:46:24	32.890	75.961	23	2.9	4
118	24-05-2016	10:17:55	30.856	74.752	26	4.1	3
119	01-08-2016	12:34:48	31.627	77.996	22	2.7	3
120	28-08-2016	12:22:41	32.241	75.896	14	2.6	6
121	02-10-2016	23:23:41	29.230	76.962	28	2.5	6
122	16-11-2016	05:07:44	31.474	75.923	44	3.7	7
123	16-11-2016	22:59:12	27.745	76.063	20	4.4	6
124	02-12-2016	22:51:02	33.514	75.802	16	3.2	5
125	14-12-2016	12:58:07	28.657	76.698	19	2.6	4
126	19-12-2016	04:31:55	30.692	77.741	32	3.2	4
127	26-12-2016	22:26:52	31.252	76.734	27	3.2	3
128	10-01-2017	15:25:43	30.709	79.671	25	3.0	3
129	23-01-2017	09:33:03	30.666	77.889	63	3.2	4
130	03-02-2017	13:35:51	30.145	78.656	30	3.4	4
131	11-02-2017	17:21:14	30.146	78.603	32	3.4	8
132	27-02-2017	16:23:52	33.406	74.866	12	2.7	7
133	01-03-2017	20:09:25	32.230	76.385	25	3.3	6
134	09-03-2017	08:39:54	32.086	75.629	4	3.3	4
135	16-04-2017	23:09:50	30.197	78.690	29	3.4	3
136	18-04-2017	05:12:00	32.666	75.508	23	4.6	3
137	27-04-2017	12:29:14	29.560	76.803	18	2.7	4
138	18-05-2017	22:08:41	33.360	76.771	17	2.5	3
139	19-05-2017	00:02:27	32.235	75.392	4	4.5	8
140	20-05-2017	05:48:40	32.229	75.391	4	4.2	10
141	20-05-2017	05:48:45	33.200	76.698	27	2.5	4
142	21-05-2017	00:41:33	33.010	76.541	23	2.5	3
143	02-06-2017	03:02:20	29.100	77.238	32	2.9	9
144	05-06-2017	14:54:33	29.844	76.902	7	2.5	7
145	14-06-2017	17:56:20	33.560	77.411	9	2.8	7
146	10-07-2017	21:38:56	30.348	78.737	8	3.5	6
147	15-07-2017	02:25:31	30.320	77.367	20	3.4	3
148	19-07-2017	13:59:35	33.779	70.919	5	3.3	3
149	10-08-2017	16:08:45	32.465	78.631	12	3.0	4
150	22-08-2017	15:22:09	30.418	78.175	17	3.7	3
151	19-09-2017	19:16:49	29.157	76.573	20	2.7	4
152	19-10-2017	00:54:25	33.500	75.910	19	3.2	4
153	19-10-2017	01:10:24	32.500	74.845	9	4.6	4
154	27-10-2017	08:54:18	31.997	75.851	20	3.6	4
155	28-10-2017	16:53:51	28.400	76.161	4	3.1	3
156	06-12-2017	15:19:52	30.431	78.551	12	4.7	3
157	28-12-2017	11:17:28	30.277	78.645	24	3.5	4

Appendix 2. Showing estimates of spectral parameters and source parameters of 157 events

SI no.	Long term spectral level (Ωo)	Corner frequency (fc) (Hz)	Maximum frequency (fmax) (Hz)	Kappa (K) (*sec*)	Seismic moment (Mo) (dyne cm)	Standard deviation (STD)	Moment magnitude (Mw)	Standard deviation (STD)	Source radius (r) (m)	Standard deviation (STD)	Stress drop (Δσ) (bars)	Standard deviation (STD)
1	4.90E+01	5.6	11.8	0.03	6.16E+19	0.12	2.5	0.01	234	0.35	2.1	0.93
2	1.83E+03	3.8	9.5	0.04	2.30E+21	0.06	3.5	0.00	346	0.47	24.3	1.35
3	1.09E+03	4.6	11.7	0.03	1.38E+21	0.28	3.4	0.02	284	0.12	26.3	0.30
4	6.64E+02	3.3	8.9	0.04	8.35E+20	0.21	3.2	0.02	397	0.22	5.8	0.44
5	1.40E+03	4.2	9.3	0.04	1.76E+21	0.33	3.5	0.03	309	0.15	26.1	0.71
6	1.32E+03	4.7	10.4	0.03	1.66E+21	0.24	3.4	0.02	277	0.20	34.1	0.65
7	1.44E+04	4.9	12.9	0.03	1.81E+22	0.29	4.1	0.02	267	0.09	17.0	0.35
8	5.39E+01	6.5	17.4	0.02	6.77E+19	0.40	2.5	0.05	201	0.03	3.7	0.48
9	1.50E+02	4.2	9.6	0.03	1.88E+20	0.25	2.8	0.03	308	0.20	2.8	0.36
10	7.51E+01	6.0	13.2	0.03	9.45E+19	0.24	2.6	0.03	218	0.31	4.0	0.89
11	1.18E+03	6.9	16.2	0.02	1.49E+21	0.42	3.4	0.03	190	0.08	94.7	0.52
12	2.10E+01	7.1	16.3	0.02	2.64E+19	0.15	2.2	0.02	183	0.09	1.9	0.43
13	6.22E+02	6.5	14.2	0.02	7.82E+20	0.39	3.2	0.03	201	0.10	41.9	0.56
14	1.15E+03	4.6	11.2	0.03	1.44E+21	0.29	3.4	0.03	286	0.04	27.1	0.38
15	2.35E+02	2.2	6.5	0.05	2.96E+20	1.26	2.9	0.12	588	0.35	0.6	1.60
16	8.16E+01	4.8	11.9	0.03	1.03E+20	0.26	2.6	0.03	270	0.39	2.3	1.04

17	8.80E+04	3.2	9.2	0.04	1.11E+23	0.32	4.7	0.02	404	0.19	69.4	0.73
18	7.33E+03	2.2	5.6	0.06	9.22E+21	0.46	3.9	0.03	580	0.08	20.7	0.31
19	3.97E+04	3.7	8.6	0.04	4.99E+22	0.41	4.4	0.03	354	0.12	73.7	0.21
20	1.12E+03	5.5	13.4	0.02	1.40E+21	0.44	3.4	0.04	236	0.12	46.7	0.52
21	6.54E+03	5.7	15.1	0.02	8.22E+21	1.43	3.8	0.13	230	0.30	54.2	1.18
22	3.77E+03	5.0	13.0	0.03	4.74E+21	1.57	3.6	0.13	259	0.16	50.3	1.24
23	3.68E+01	5.8	15.1	0.02	4.62E+19	0.23	2.4	0.03	223	0.08	1.8	0.11
24	1.53E+03	4.0	9.0	0.04	1.92E+21	0.23	3.5	0.02	325	0.23	24.5	0.48
25	1.27E+03	3.6	9.0	0.04	1.59E+21	0.48	3.4	0.04	363	0.19	14.6	0.43
26	2.39E+01	4.8	9.3	0.04	3.00E+19	0.39	2.3	0.05	271	0.23	0.7	1.07
27	1.58E+03	5.0	13.8	0.02	1.98E+21	0.23	3.5	0.02	260	0.20	49.4	0.37
28	8.54E+02	5.5	11.7	0.03	1.07E+20	0.37	3.3	0.03	239	0.09	34.3	0.16
29	1.11E+02	3.4	7.7	0.04	1.40E+20	0.15	2.7	0.02	382	0.22	1.1	0.65
30	1.19E+03	7.4	17.1	0.02	1.50E+21	0.76	3.4	0.07	175	0.12	73.3	0.93
31	3.63E+01	3.6	9.0	0.04	4.56E+19	0.33	2.4	0.04	365	0.29	0.4	0.55
32	2.18E+03	3.4	9.9	0.03	2.74E+21	0.41	3.6	0.03	387	0.28	20.6	0.69
33	4.04E+02	3.7	9.2	0.04	5.08E+20	0.38	3.1	0.03	353	0.25	5.0	0.49
34	2.15E+03	4.6	14.7	0.02	2.70E+21	0.30	3.6	0.02	282	0.12	52.8	0.30
35	6.32E+01	5.1	11.9	0.03	7.95E+19	0.34	2.6	0.04	256	0.35	2.1	1.24
36	6.72E+02	3.3	8.2	0.04	8.45E+20	0.28	3.2	0.02	393	0.27	6.1	1.02
37	6.43E+01	6.6	14.7	0.02	8.08E+19	0.41	2.6	0.05	196	0.21	4.7	0.86
38	1.55E+03	3.8	9.1	0.04	1.95E+21	0.27	3.5	0.02	342	0.20	21.3	0.60
39	1.80E+03	3.5	9.3	0.04	2.27E+21	0.04	3.5	0.00	373	0.31	19.2	0.92
40	4.05E+03	2.8	7.6	0.04	5.09E+21	0.77	3.7	0.06	473	0.35	21.0	1.41
41	4.81E+01	5.2	13.2	0.03	6.05E+19	0.17	2.5	0.02	252	0.40	1.7	1.37
42	1.42E+03	3.1	7.9	0.04	1.79E+21	0.91	3.4	0.07	414	0.23	11.0	0.87
43	8.37E+03	2.3	7.1	0.05	1.05E+22	1.34	3.9	0.12	561	0.28	26.0	0.73
44	2.71E+04	1.6	5.2	0.06	3.41E+22	0.26	4.3	0.02	798	0.15	29.3	0.55
45	7.04E+02	3.7	8.5	0.04	8.85E+20	0.50	3.3	0.04	353	0.24	8.8	0.54
46	1.61E+03	2.8	7.3	0.05	2.03E+21	0.65	3.5	0.05	466	0.09	8.8	0.37
47	1.85E+03	2.4	11.4	0.03	2.32E+21	0.10	3.5	0.01	540	0.21	6.4	0.52
48	7.25E+02	3.7	9.5	0.04	9.12E+20	0.86	3.2	0.09	353	0.25	9.0	0.58
49	3.08E+02	3.5	6.7	0.05	3.87E+20	0.38	3.0	0.04	377	0.18	3.2	0.17
50	2.67E+03	5.0	11.4	0.03	3.35E+21	0.54	3.6	0.04	262	0.27	81.5	0.79
51	2.55E+03	4.1	8.1	0.04	3.21E+21	0.75	3.6	0.06	318	0.20	43.7	0.16
52	1.27E+03	2.1	5.2	0.06	1.60E+21	0.20	3.4	0.02	620	0.07	2.9	0.02
53	4.54E+04	2.9	8.8	0.04	5.71E+22	0.38	4.5	0.02	453	0.13	10.8	0.28
54	2.08E+03	3.6	9.8	0.03	2.61E+21	0.55	3.6	0.05	363	0.32	23.9	1.31
55	3.25E+02	2.9	7.0	0.05	4.09E+20	0.67	3.0	0.07	450	0.16	2.0	0.26
56	1.32E+03	3.3	9.2	0.04	1.65E+21	2.32	3.2	0.21	391	0.14	12.1	1.98
57	6.74E+03	3.1	8.1	0.04	8.47E+21	1.00	3.9	0.08	422	0.23	49.2	0.89
58	2.44E+03	5.5	16.4	0.02	3.07E+21	0.35	3.6	0.03	239	0.18	98.7	0.75
59	1.96E+02	6.5	14.2	0.02	2.46E+20	0.18	2.9	0.02	201	0.08	13.3	0.35
60	1.96E+03	4.6	13.9	0.02	2.47E+21	0.07	3.6	0.01	284	0.05	47.2	0.11
61	2.76E+03	4.6	12.5	0.03	3.47E+21	0.50	3.7	0.04	283	0.08	67.1	0.76
62	4.09E+01	3.9	9.1	0.04	5.14E+19	0.27	2.4	0.03	336	0.27	0.6	0.68
63	7.66E+02	4.2	11.8	0.03	9.63E+20	0.35	3.3	0.03	308	0.09	14.4	0.23
64	1.02E+02	2.5	6.7	0.05	1.28E+20	0.28	2.7	0.03	526	0.26	0.4	0.43
65	6.12E+03	1.6	5.2	0.06	7.70E+21	0.49	3.9	0.04	826	0.23	6.0	0.22
66	1.89E+03	3.6	6.7	0.05	2.37E+21	0.46	3.5	0.04	360	0.09	22.3	0.31
67	8.38E+01	7.0	18.7	0.02	1.05E+20	0.71	2.6	0.08	187	0.25	7.1	0.03
68	1.45E+02	5.0	10.3	0.03	1.82E+20	0.11	2.8	0.01	260	0.33	4.5	0.89
69	2.65E+04	3.1	7.4	0.05	3.33E+22	0.49	4.3	0.03	423	0.02	71.0	0.55
70	2.63E+04	3.2	9.7	0.03	3.31E+22	0.44	4.3	0.03	408	0.15	25.7	0.29
71	5.08E+01	3.5	9.8	0.03	6.39E+19	0.18	2.5	0.02	371	0.30	0.6	0.92
72	1.85E+05	1.3	5.1	0.07	2.32E+23	0.42	4.9	0.02	975	0.16	95.3	0.45
73	2.86E+04	2.9	8.8	0.04	3.59E+22	0.45	4.3	0.03	446	0.14	37.6	0.47
74	1.88E+03	2.4	9.3	0.04	2.36E+21	0.31	3.5	0.03	546	0.15	6.3	0.14
75	3.25E+02	3.7	9.8	0.03	4.08E+20	0.32	3.0	0.03	350	0.31	4.2	0.87
76	3.48E+03	1.6	5.6	0.06	4.37E+21	0.54	3.7	0.04	792	0.03	3.9	0.46
77	2.23E+03	5.1	11.5	0.03	2.81E+21	0.81	3.6	0.06	257	0.32	72.3	0.95
78	3.88E+02	3.2	7.8	0.04	4.87E+20	0.17	3.1	0.02	401	0.14	3.3	0.54
79	3.55E+03	3.8	10.8	0.03	4.47E+21	1.44	3.6	0.12	339	0.29	50.3	1.51
80	1.57E+03	3.1	8.0	0.04	1.97E+21	0.28	3.5	0.02	422	0.37	11.5	1.09
81	5.34E+04	3.2	9.9	0.03	6.71E+22	0.14	4.5	0.01	401	0.02	99.9	0.08
82	4.19E+02	3.6	7.9	0.04	5.27E+20	0.58	3.1	0.05	366	0.30	4.7	1.44
83	1.20E+03	3.6	9.3	0.04	1.51E+21	0.40	3.4	0.03	364	0.21	13.7	0.80
84	8.92E+03	2.9	11.1	0.03	1.12E+22	0.13	4.0	0.01	446	0.17	55.2	0.64
85	8.57E+01	5.4	13.2	0.03	1.08E+20	0.23	2.7	0.03	242	0.35	3.3	0.89
86	2.41E+02	5.7	19.4	0.02	3.03E+20	1.62	2.8	0.19	228	0.33	11.2	0.67
87	5.82E+01	7.6	30.1	0.01	7.32E+19	1.61	2.4	0.17	172	0.41	6.3	0.30
88	3.45E+02	4.7	32.8	0.01	4.33E+20	0.55	3.0	0.05	277	0.02	8.9	1.09
89	4.77E+02	8.0	25.4	0.01	6.00E+19	1.19	3.1	0.11	163	0.29	6.1	0.31
90	2.30E+02	7.2	40.3	0.01	5.89E+20	0.60	2.9	0.05	181	0.52	43.4	0.01
91	3.07E+02	5.9	18.5	0.02	3.87E+20	0.26	3.0	0.03	222	0.24	15.5	1.62
92	7.41E+02	4.5	17.7	0.02	9.31E+20	0.77	3.3	0.07	292	0.35	16.4	0.22
93	6.42E+02	4.8	11.9	0.03	8.08E+20	0.57	3.2	0.05	269	0.21	18.2	0.05
94	4.23E+02	7.5	21.5	0.02	5.30E+20	1.52	3.0	0.16	173	0.31	44.9	0.70
95	1.41E+03	6.2	16.1	0.02	1.77E+21	1.16	3.4	0.10	211	0.51	82.9	0.65
96	9.24E+02	6.4	18.8	0.02	1.16E+21	1.16	3.3	0.10	203	0.29	60.5	0.70

97	1.79E+02	8.0	28.3	0.01	1.25E+20	0.80	2.8	0.08	163	0.23	12.6	0.76
98	7.22E+04	3.5	11.6	0.03	9.07E+22	0.06	4.6	0.00	372	0.07	36.6	0.26
99	1.34E+03	5.4	10.9	0.03	1.68E+21	0.35	3.4	0.03	241	0.06	52.4	0.92
100	5.37E+03	4.7	18.4	0.02	6.76E+20	0.61	3.8	0.05	277	0.24	13.9	0.47
101	1.38E+03	6.4	20.0	0.02	1.74E+21	1.81	3.3	0.18	202	0.24	91.9	0.13
102	3.32E+02	8.5	28.7	0.01	4.18E+19	1.18	3.0	0.12	153	0.40	5.1	0.16
103	5.92E+02	6.6	11.6	0.03	7.44E+20	1.84	3.0	0.19	198	0.35	42.2	0.34
104	2.60E+01	8.7	10.8	0.03	3.28E+19	0.93	2.3	0.13	150	0.46	4.3	1.62
105	8.83E+02	6.5	20.4	0.02	1.11E+21	0.92	3.3	0.08	202	0.61	59.3	0.80
106	3.49E+03	4.5	18.5	0.02	4.38E+21	0.95	3.7	0.07	289	0.34	8.0	0.66
107	3.85E+02	4.6	14.1	0.03	4.84E+20	0.98	3.0	0.10	284	0.16	9.2	1.09
108	4.56E+02	7.1	13.4	0.02	5.73E+20	1.30	3.0	0.13	184	0.16	40.5	0.34
109	2.35E+02	8.8	28.3	0.01	2.96E+19	1.00	2.9	0.10	148	0.22	40.0	0.51
110	1.06E+02	7.5	21.2	0.02	1.33E+20	1.84	2.6	0.20	174	0.54	11.1	0.59
111	4.54E+02	5.3	15.3	0.01	5.71E+20	0.05	3.1	0.15	246	0.01	16.7	0.22
112	5.50E+01	8.1	15.8	0.01	6.92E+19	2.47	2.2	0.14	161	0.54	7.3	1.02
113	1.15E+02	4.3	12.6	0.02	1.45E+20	0.12	2.7	0.00	306	0.10	2.2	1.96
114	1.90E+02	5.5	24.4	0.02	2.39E+20	0.98	2.8	0.31	237	0.10	7.9	0.66
115	1.02E+04	2.9	15.6	0.03	1.27E+22	0.36	4.0	0.11	450	0.10	61.3	0.30
116	7.12E+02	3.9	10.3	0.01	8.95E+20	0.05	3.3	0.10	332	0.16	10.8	0.77
117	5.27E+02	6.8	17.2	0.02	6.65E+20	1.13	3.1	0.03	191	0.20	41.6	0.01
118	7.45E+03	3.6	13.5	0.03	9.36E+21	0.28	3.9	0.04	365	0.06	84.5	1.22
119	3.49E+03	4.8	13.3	0.02	4.40E+21	0.22	3.7	0.10	274	0.57	93.5	1.41
120	1.07E+03	5.6	14.8	0.02	1.35E+21	0.85	3.4	0.02	231	0.17	47.7	0.21
121	2.03E+02	5.8	15.0	0.03	2.56E+20	0.11	2.8	0.02	224	0.24	10.0	0.59
122	2.24E+03	5.6	20.1	0.02	2.82E+20	1.30	3.0	0.07	233	0.24	9.8	1.62
123	1.74E+04	2.8	9.7	0.02	2.18E+22	0.01	4.2	0.16	466	0.18	94.6	1.42
124	6.75E+02	4.8	18.9	0.02	8.50E+20	0.13	3.3	0.15	274	0.38	18.0	0.06
125	3.01E+03	4.6	23.6	0.04	3.78E+21	1.56	3.8	0.03	284	0.75	72.6	1.49
126	9.11E+02	7.4	19.6	0.02	1.15E+21	1.18	3.3	0.01	176	0.35	91.8	1.11
127	2.58E+03	4.6	14.9	0.01	3.24E+21	1.13	3.6	0.11	282	0.17	60.9	0.92
128	3.10E+02	5.5	12.2	0.02	3.90E+20	2.26	2.2	0.11	237	227.93	12.8	0.47
129	9.88E+02	4.1	11.9	0.02	1.24E+21	1.50	3.2	0.11	319	0.41	39.1	0.34
130	2.44E+03	4.5	12.9	0.03	3.06E+21	1.16	3.5	0.51	289	0.18	57.3	0.92
131	2.62E+02	6.7	13.6	0.03	3.28E+20	1.64	2.6	0.14	193	0.29	19.9	0.06
132	6.17E+02	5.7	13.5	0.02	7.77E+20	1.68	3.0	0.11	228	0.40	29.5	1.68
133	1.06E+03	5.1	14.2	0.03	1.34E+21	1.22	3.3	0.30	254	0.23	35.6	1.16
134	3.07E+02	5.4	9.4	0.02	3.86E+20	1.55	2.8	0.20	242	0.38	12.0	1.52
135	7.52E+02	4.1	12.9	0.02	9.44E+20	1.50	3.1	0.12	317	0.26	13.0	1.42
136	3.97E+03	4.2	14.5	0.03	4.99E+21	1.21	3.6	0.13	313	0.23	71.3	0.65
137	6.27E+02	6.1	17.0	0.03	7.89E+20	0.94	3.2	0.13	214	0.31	35.1	0.34
138	2.44E+02	5.5	13.2	0.02	3.07E+20	1.51	2.8	0.11	236	0.40	26.4	1.13
139	2.33E+03	3.6	11.6	0.02	2.93E+21	1.56	3.4	0.08	366	0.27	59.4	0.30
140	2.00E+03	3.9	12.2	0.03	2.51E+21	1.18	3.5	0.15	333	0.26	29.7	0.36
141	3.65E+02	4.5	11.4	0.03	4.59E+20	1.12	3.0	0.15	290	0.18	8.3	0.66
142	2.64E+02	6.9	17.6	0.03	3.32E+20	1.87	2.7	0.11	190	0.28	21.3	1.13
143	6.72E+02	7.6	21.1	0.02	8.45E+20	1.26	3.2	0.19	171	0.30	74.1	0.06
144	7.61E+02	6.8	16.8	0.02	9.57E+20	1.22	3.2	0.11	192	0.43	58.4	0.92
145	7.66E+01	6.8	13.3	0.02	9.64E+19	1.35	2.5	0.08	192	0.29	6.0	0.16
146	1.47E+03	5.0	15.6	0.02	1.85E+21	1.50	3.3	0.14	262	0.16	44.5	0.34
147	1.54E+03	5.0	12.6	0.03	1.93E+21	1.62	3.3	0.19	261	0.16	47.5	0.70
148	6.96E+01	8.3	14.7	0.02	8.74E+19	2.31	2.6	0.18	157	0.16	9.9	1.09
149	5.76E+02	8.6	20.1	0.03	7.25E+20	1.64	3.0	0.14	152	0.16	90.0	1.11
150	4.43E+03	3.6	11.1	0.02	5.57E+21	0.96	3.7	0.12	365	0.20	50.3	0.92
151	2.15E+02	5.6	10.8	0.02	2.70E+20	2.32	2.4	0.16	233	0.40	9.3	1.09
152	3.89E+03	3.3	10.2	0.03	4.89E+21	0.88	3.7	0.13	391	0.28	36.3	0.34
153	9.62E+02	3.9	8.1	0.03	1.21E+21	1.56	3.2	0.03	332	0.42	30.9	0.30
154	5.72E+02	4.6	12.1	0.03	7.19E+20	1.81	2.9	0.11	282	0.22	41.0	0.34
155	7.31E+02	4.8	12.7	0.04	9.18E+20	2.29	2.8	0.14	270	0.56	68.8	0.50
156	5.05E+04	7.8	12.6	0.03	6.34E+19	1.28	4.4	0.02	167	0.38	5.9	0.66
157	5.00E+03	4.5	12.4	0.03	6.28E+21	1.71	3.7	0.04	291	0.23	69.5	1.18

References

Abercrombie, R.E., 1995. Earthquake source scaling relationships from 1 to 5 ML using seismograms recorded at 2.5 km depth. J. Geophys. Res. 100, 24015–24036.

Abercrombie, R.E., Leary, P.C., 1993. Source parameters of small earthquakes recorded at 2.5 km depth, Cajon Pass, southern California: implications for earthquake scaling. Geophys. Res. Lett. 20, 1511–1514.

Aki, K, 1967. Scaling law of seismic spectrum. J Geophys. Res. 72 (4), 1217 1231.

Aki, K., 1987. Magnitude-frequency relation for small earthquakes: A clue to the origin of f_{max} of large earthquakes. J. Geophys. Res. 92, 1349–1355.

Anderson, J.G., 1986. Implication of attenuation for studies of the earthquake source. In: Das, S., Boatwright, J., Scholz, C.H. (Eds.), Earthquake Source Mechanics, Maurice Ewing Series 6. American Geophysical Union, Washington, D.C., pp. 311–318.

Anderson, J.G., 1991. A preliminary descriptive model for the distance dependence of the spectral decay parameter in southern California. Bull. Seism. Soc. Am. 81, 2186–2193.

Anderson, J.G., Hough, S.E., 1984. A model for the shape of the Fourier amplitude spectrum of acceleration at high frequencies. Bull. Seism. Soc. Am. 74, 1969–1993.

Andrews, D.J., 1986. Objective determination of source parameters and similarity of earthquakes of different size. In: Das, S., Boatwright, J., Sholtz, C.H. (Eds.), Earthquake Source Mechanics. American Geophysical Union, Washington, D.C., pp. 259–268.

Archuleta, R.J., Cranswick, E., Mueller, C., Spudich, P., 1982. Source parameters of the 1980 Mammoth lakes, California, earthquakes sequence. J. Geophys. Res. 87 (B6), 4595–4607.

Arita, K., 1983. Origin of the inverted metamorphism of the Lower Himalaya, central Nepal. Tectonophysics 95, 43–60.

Bansal, B. K., 1998. Determination of source parameters for small earthquake in the Koyna region. 11th Symposium on Earthquake Engineering, Roorkee, 57-66.

Bindi, D., Spallarossa, D., Augliera, P., Cattaneo, M., 2001. Source parameters estimated from the aftershocks of the 1997 Umbria-Marche (Italy) seismic sequence. Bull. Seismol. Soc. Am. 91, 448–455.

Brune, J.N., 1970. Tectonic stress and the spectra of seismic shear waves from

earthquakes. J. Geophys. Res. 75, 4997–5009.
Brune, J.N., 1971. Correction to tectonic stress and the spectra of seismic shear waves from earthquakes. J. Geophys. Res. 76, 5002.
Burg, J.P., Leyreloup, A., Girardeau, J., Chen, G.M., 1987. Structure and metamorphism of a tectonically thickened continental crust—the Yalu Tsangpo suture zone (Tibet). Philos. Trans. R. Soc. Lond. Ser. A 321, 67–86.
Campillo, M., 1983. Numerical evaluation of near-field, high-frequency radiation from quasi-dynamic circular faults. Bull. Seism. Soc. Am. 73, 723–734.
Cantore, L., Oth, A., Parolai, S., Bindi, D., 2011. Attenuation, source parameters and site effects in the Irpinia-Basilicata region (southern Apennines, Italy). J. Seismol. 15, 375–389. https://doi.org/10.1007/s10950-011-9230-2.
Chandler, A.M., Lam, N.T.K., Tsang, H.H., 2006a. Regional and local factors in attenuation modelling: Hong Kong case study. J. Asian Earth Sci. 27, 892–906.
Chandler, A.M., Lam, N.T.K., Tsang, H.H., 2006b. Near surface attenuation modelling based on rock shear wave velocity profile. Soil Dynam. Earthq. Eng. 26, 1004–1014.
Faccioli, E., 1986. A study of spectra and peak values of strong motion accelerograms from Italy and Yugoslavia in terms of gross source properties. In: Das, S., Boatwright, J., Scholz, C.H. (Eds.), Earthquake Source Mechanics, Geophysical Monograph 37, Maurice Ewing Series, vol. 6. American Geophysical Union, Washington, D.C., pp. 297–310.
Fletcher, J.B., 1980. Spectra for high dynamic range digital recordings of Oroville, California aftershocks and their source parameters. Bull. Seism. Soc. Am. 70, 735–755.
Fujiwara, H., Irikura, K., 1991. High-frequency seismic wave radiation from antiplane cohesive zone model and f_{max} as source effect. Bull. Seism. Soc. Am. 81 (4), 1115–1128.
Ganser, A., 1964. Geology of the Himalayas. Interscience, London 289.
Gupta, I.D., Rambabu, V., 1993. Source parameters of some significant earthquakes near Koynadam. India. Pure Appl. Geophysics 140 (3), 403–413.
Hanks, T.C., 1982. f_{max}. Bull. Seism. Soc. Am. 72, 1869–1879.
Hanks, T.C., Boore, D.M., 1984. Moment-magnitude relations in theory and practice. J. Geophys. Res. 89, 6229–6235.
Hanks, T.C., Kanamori, H., 1979. A moment magnitude scale. J. Geophys. Res. 84, 2348–2350.
He, P., Lei, J., Yuan, X., Xu, X., Xu, Q., Liu, Z., Mi, Q., Lianqing, Z., 2018. Lateral Moho variations and the geometry of the Main Himalayan Thrust beneath the Nepal Himalayan orogen revealed by teleseismic receiver functions. Geophys. J. Int. 214 (2), 1004–1017.
Hiramatsu, Y., Yamanaka, H., Tadokoro, K., Nishigami, K., Ohmi, S., 2002. Scaling law between corner frequency and seismic moment of microearthquakes: is the breakdown of the cube law a nature of earthquakes? J. Geophys. Lett. 29 (8), 1211. https://doi.org/10.1029/2001GL013894.
Huang, J., Dapeng, Z., 2006. High-resolution mantle tomography of China and surrounding regions. J. Geophys. Res. 111. https://doi.org/10.1029/2005JB004066.
Izutani, Y., Kanamori, H., 2001. Scale-dependence of seismic energy-to-moment ratio for strike-slip earthquakes in Japan. Geophys. Res. Lett. 28, 4007–4010.
Kanamori, H., Anderson, D.L., 1975. Theoretical basis of some empirical relations in seismology. Bull. Seism. Soc. Am. 65, 1073–1095.
Kanamori, H., Rivera, L., 2004. Static and dynamic scaling relations for earthquakes and their implications for rupture speed and stress drop. Bulletin of Seismological Society of America 94, 314–319.
Khattri, K.N., Chander, R., Gaur, V.K., Sarkar, I., Kumar, S., 1989. New seismological results on the tectonics of the Garhwal Himalaya, Proceedings of the Indian Academy of Sciences (Earth and Planetary sciences). Bull. Seism. Soc. Am. 98 (1), 91–109.
Kinoshita, S., 1992. Local characteristics of the f_{max} of bedrock motion in the Tokyo metropolitan area, Japan. Journal of Physics of the Earth 40, 487–515.
Kumar, A., 2011. Study of earthquake source parameters using microearthquakes and strong motion data. Ph.D Thesis, Indian Institute of Technology, Roorkee.
Kumar, A., Pandey, A.D., Sharma, M.L., Gupta, S.C., Verma, A.K., Gupta, B.K., 1994. Processing and Preliminary Interpretation of Digital Data Obtained From Digital Telemetered Seismic Array in the Garhwal Himalaya, Xth Symposium on Earthquake Engineering. University of Roorkee Nov. 16-18, 1994.
Kumar, A, Gupta, SC, Kumar, A, Sen, A, Jindal, A K, Jain, S., 2006a. Estimation of source parameters from local earthquakes in Western part of the Arunachal Lesser Himalaya. 3[th]Symposium on Earthquake Engineering, 9–17.
Kumar, D., Sriram, V., Khattri, K.N., 2006b. A study of source parameters, site amplification functions and average effective shear wave quality factor Qseff from analysis of accelerograms of the 1999 Chamoli earthquake. Himalaya. Pure App. Geophys. 163, 1369–1398.
Kumar, D., Sriram, V., Sarkar, I., Teotia, S.S., 2008. An estimate of a scaling law of seismic spectrum for earthquakes in Himalaya. Indian Minerals 61 (3–4) & 62 (1–4), 83–92.
Kumar, A., Kumar, A., Mittal, H., Kumar, A., Bhardwaj, R., 2012a. Software to estimate earthquake spectral and source parameters. Int. J. Geosci. 3, 1142–1149.
Kumar, A., Mittal, H., Sachdeva, R., Kumar, A., 2012b. Indian national strong motion network. Seism. Res. Lett. 83 (1), 59–66.
Kumar, A., Kumar, A., Mittal, H., 2013a. Earthquake source parameters –review Indian context. Research and Development (IJCSEIERD) 3 (1), 41–52.
Kumar, A., Kumar, A., Gupta, S.C., Mittal, H., Kumar, R., 2013b. Source parameters and f_{max} in Kameng region of Arunachal Lesser Himalaya. J. Asian Earth Sci. 70-71, 35–44.
Kumar, A., Kumar, A., Gupta, S.C., Jindal, A.K., Ghangas, V., 2014a. Seismicity and source parameters of local earthquakes in Bilaspur region of Himachal Lesser Himalaya. Arab. J. Geosci. 7 (6), 2257–2267.
Kumar, A, Mittal, H, Kumar, R, Ghangas, V., 2014b. High frequency cut-off of observed earthquake spectrum and source parameters of local earthquakes in Himachal Himalaya. International Journal of Science and Research 3 ISSN (online), 2319-7064.
Kumar, R., Gupta, S.C., Kumar, A., 2015. Attenuation characteristics of seismic body waves for the crust of Lower Siang region of Arunachal Himalaya. Int. J. Adv. Res. 2 (6), 742–755.
Kumar, V., Kumar, D., Chopra, S., 2016. Estimation of source parameters and scaling relations for moderate size earthquakes in NW Himalaya. J. Asian Earth Sci. 128, 79–89.
Lei, J., Xie, F., Mishra, O.P., Zhang, G., Lu, Y., Li, Y., 2012. The 2011 Yingjiang, China, earthquake (M 5.8): A volcano-related fluid-driven earthquake? Bull. Seismol. Soc. Am. 102, 417–425.
Mandal, P., Johnston, A., 2006. Estimation of source parameters for the aftershocks of the 2001 Mw 7.7 Bhuj Earthquake. India, Pure Appl. Geophys. 163, 1537–1560.
Mandal, P., Rastogi, B.K., 1998. A frequency-dependent relation of coda Q_c for Koyna Warna region. India. Pure Appl. Geophys. 153, 163–177.
Mcgarr, A., 1980. Some constraints on levels of shear stress in the crust from observations and theory. J. Geophys. Res. 85, 6231–6238.
Mishra, O.P., 2012. Seismological Research in India. Proceedings of Indian National Science. Academy Publication (PINSA) 76 (3), 361–375.
Mishra, O.P., 2013. Crustal heterogeneity in bulk velocity beneath the 2001 Bhuj earthquake source zone and its implications. Bull. Seismol. Soc. Am. 103 (6), 3235–3247. https://doi.org/10.1785/0120110144.
Mishra, O.P., 2014. Intricacies of Himalayan seismotectonics and seismogenesis: need of an integrated research. Curr. Sci. 106 (2), 176–187.
Mishra, O.P., Zhao, D., 2003. Crack density, saturation rate and porosity at the 2001 Bhuj, India, earthquake hypocenter: a fluid-driven earthquake? Earth planet. Sci. Lett. 212, 393–405.
Mishra, O.P., Zhao, D., Singh, D.D., 2005a. Surface-wave studies beneath the Pacific Ocean. Bull. Seismolog. Soc. Am. 95 (6), 2152–2161.
Mishra, O.P., Zhao, D., Singh, D.D., 2005b. Northwest Pacific fundamental mode Rayleigh-wave group velocity and its relationship with tectonic structures. Bull. Seismolog. Soc. Am. 95 (6), 2125–2135.
Mishra, O.P., Zhao, D., Wang, Z., 2008. The genesis of the 2001 Bhuj, India, earthquake (Mw 7.6): a puzzle for peninsular India. J Indian Miner (Special Issue) 61(3–4) & 62 (1–4), 149–170.
Morikawa, N., Sasatani, T., 2000. The 1994 Hokkaido Toho-oki earthquake sequence: the complex activity of intra-slab and plate-boundary earthquakes. Phys. Earth Planet. Inter. 121 (1), 39–58.
Nakata, T., 1989. Active faults of the Himalaya of India and Nepal. Geol. Soc. Am. Pap. 232, 243–264.
Ni, J., Barazangi, M., 1984. Seismotectonics of the Himalayan collision zone: geometry of the underthrusting Indian plate beneath the Himalaya. J. Geophys. Res. 89, 1132–1146.
O'Neill, M.E., 1984. Source dimensions and stress drops of small earthquakes near Parkfield. California. Bull. Seism. Soc. Am. 71, 27–40.
Paidi, V., Kumar, A., Gupta, S.C., Kumar, A., 2015. Estimation of source parameters of local earthquakes in the environs of Koldam site. Arab. J. Geosci. https://doi.org/10.1007/s12517-013-1212-y.
Papageorgiou, A.S., 1988. On two characteristic frequencies of acceleration spectra: patch corner frequency and f_{max}. Bull. Seism. Soc. Am. 78, 509–529.
Papageorgiou, A.S., Aki, K., 1983a. A specific barrier model for the quantitative description of inhomogeneous faulting and the prediction of strong around motion. I. Description of the model. Bull. Seism. Soc. Am. 73, 693–722.
Papageorgiou, A.S., Aki, K., 1983b. A specific barrier model for the quantitative description of inhomogeneous faulting and the prediction of strong ground motion. I1. Application of the model. Bull. Seism. Soc. Am. 73, 953–978.
Parshad, R., Snehmani, Rani R., Ghanghas, V., Kumar, A., Rana, V., Joshi, P., Shrivastva, P. K., Ganju, A., 2014. Source parameters of local earthquakes in Nubra region, NW Himalaya. Int. J. Adv. Res. 2, 151–158.
Prejean, S.G., Ellsworth, W.L., 2001. Observations of earthquake source parameters at 2 km depth in the Long Valley Caldera, eastern California. Bull. Seism. Soc. Am. 91 (2), 165–177.
Purvance, M.D., Anderson, J.G., 2003. A comprehensive study of the observed spectral decay in strong-motion accelerations recorded in Guerrero. Mexico. Bull. Seism. Soc. Am. 93 (2), 600–611.
Sairam, B, Singh, A. P., Ravi Kumar, M., 2018. Comparison of earthquake source characteristics in the Kachchh Rift Basin and Saurashtra horst, Deccan Volcanic Province, western India. Journal of Earth System Science 127(55), https://doi.org/10.1007/s12040-018-0957-9
Seeber, L., Armbruster, J.G., Quitt-meyer, R.C., 1981. Seismicity and continental subduction in the Himalayan arc. In Zagros, Hindu-Kush, Himalaya. Geodynamic Evolution, Geodyn. Am. Geophys. Union 3, 215–242.
Sharma, B., 2014. A comparative attenuation study of seismic waves in terms of seismic Albedo for Chamoli, Kachchh and Koyna regions of India. International Journal of Engineering Science Invention ISSN 3 (6), 33–40.
Sharma, M.L., Wason, H.R., 1994. Occurrence of low stress drop earthquakes in the Garwal Himalayan region. Physics of the Earth and Plantary Interiors 85, 265–272.
Sibson, R.H., 1974. Frictional constraints on thrust, wrench and normal faults. Nature 249, 542–544.
Singh, A.P., Mishra, O.P., Yadav, R.B.S., Kumar, D., 2012. A new insight into Crustal Heterogeneity beneath the 2001 Bhuj earthquake region of Northwest India and its implications for rupture initiations. J. Asian Earth Sci. 48, 31–42. https://doi.org/10.1016/j.jseaes.2011.12.020.
Singh, A.P., Mishra, O.P., Rastogi, B.K., Kumar, S., 2013. Crustal heterogeneities beneath the 2011 Talala, Saurashtraearthquake, Gujarat, India Source zone: Seismological Evidence for Neo-tectonics. J. Asian Earth Sci. 62, 672–689.
Tsai, C.C.P., Chen, K.C., 2000. A model for the high-cut process of strong-motion accelerations in terms of distance, magnitude, and site condition: an example from the

SMART 1 array, Lotung, Taiwan. Bull. Seism. Soc. Am. 90 (6), 1535–1542.
Tucker, B.E., Brune, J.N., 1977. Source mechanism and mb - Msanalysis of aftershocks of the San Fernando earthquake. Geophys. J. R. Astr. Soc. 49, 371–426.
Tusa, G., Langer, H., Brancato, A., Gresta, S., 2012. High-frequency spectral decay in P-wave acceleration spectra and source parameters of microearthquakes in south-eastern Sicily. Italy. Bull. Seis. Soc. Am 102, 1796–1809.
Valdiya, K.S., 1979. An outline of the structural set-up of the Kumaon Himalaya. J. Geol. Soc. India 20, 145–157.
Valdiya, K.S., 1987. Trans-Himadri Thrust and domalupwarps immediately south of collision zone and tectonic implications. Curr. Sci. 56, 200–209.
Valdiya, K. S., 1989. Trans-Himadri intra crustal fault and basement upwarps south of the Indus-Tsangpo Suture Zone. Geol. Soc. Amer. Spec.,153–168.
Valdiya, K.S., 1998. Dynamic Himalaya 178. Univ, Press, Hyderabad, India.
Valdiya, K.S., Joshi, D.D., Sanwal, R., Tandon, S.K., 1984. Geomorphologic envelopment across the active main boundary Thrust, an example from the Nainital Hills in Kumaun Himalaya. J. Geol. Soc. India 25 (12), 761–774.
Vandana, Mishra, O. P., 2018. Seismic Attenuation characteristics of Northwest Himalaya and its surrounding region and their implications to structural heterogeneities and seismogenesis (Under review).
Vandana, Kumar, A., Gupta, S.C., 2016a. Attenuation characteristics of body waves for the Bilaspur region of Himachal Lesser Himalaya. Pure Appl. Geophys. 173, 447–462.
Vandana, Gupta, S.C., Kumar, A., 2016b. Coda wave attenuation characteristics for the Bilaspur region of Himachal Lesser Himalaya. Natural Hazard 78 (2), 1091–1110.
Vandana, Kumar, A., Gupta, S.C., Mishra, O.P., Kumar, A., Sandeep, 2017. Source parameters and high frequency characteristics of local events ($0.5 \leq M_L \leq 2.9$) around Bilaspur Region of the Himachal Himalaya. Pure Appl. Geophys. 174, 1643–1658.
Venkataraman, A., Beroza, G.C., Ide, S., Imanishi, K., Ito, H., Iio, Y., 2006. Measurements of spectral similarity for microearthquakes in western Nagano. Japan. J. Geophys. Res. 111, B03303. https://doi.org/10.1029/2005JB003834.
Wen, J., Chen, X., 2012. Variations in f_{max} along the ruptured fault during the Mw 7.9 Wenchuan earthquake of 12 May 2008. Bull. Seism. Soc. Am. 102 (3), 991–998.
Yin, A., Harrison, T.M., 2000. Geologic evolution of the Himalayan-Tibetan orogen. Annu. Rev. Earth Planet. Sci. 28, 211–280.
Yokoi, T., Irikura, K., 1991. Meaning of source controlled f_{max} in empirical Green's function technique based on a T^2-scaling law, Annuals of Disaster Prevention Research Institute. Kyoto University 34 B-1, 177-189.
Zhou, Z., Lei, J., 2016. Pn anisotropic tomography and mantle dynamics beneath China. ⇑ Physics of the Earth and Planetary Interiors 257, 193–204.
Zobin, V.M., Havskov, J., 1995. Source spectral properties of small earthquakes in the northern North Sea. Tectonophysics 248, 207–218.